Nat. Hazards Earth Syst. Sci. Discuss., https://doi.org/10.5194/nhess-2018-271
Manuscript under review for journal Nat. Hazards Earth Syst. Sci.
Discussion started: 13 November 2018

Natural Hazards and Earth System Sciences
Discussions

Simple rules to minimize exposure to coseismic landslide hazard

David G. Milledge[1], Alexander L. Densmore[2], Dino Bellugi[3], Nick J. Rosser[2], Jack Watt[2], Gen Li[4], Katie J. Oven[2]

1. School of Engineering, Newcastle University, Newcastle upon Tyne, UK

2. Institute of Hazard, Risk, and Resilience and Department of Geography, Durham University, Durham, UK

3. Department of Geography, University of California, Berkeley, USA

4. Department of Earth Sciences, University of Southern California, Los Angeles, USA

Abstract

Landslides constitute a hazard to life and infrastructure, and their risk is mitigated primarily by reducing exposure. This requires information on landslide hazard at a scale that can enable informed decisions about how to respond to that hazard. Such information is often unavailable to, or not easily interpreted by, those who might need it most (e.g., householders, local government, and NGOs). To address this shortcoming, we develop simple rules to identify landslide hazard that are understandable, communicable, and memorable, and that require no prior knowledge, skills, or equipment to evaluate. We examine rules based on two common metrics of landslide hazard, local slope and upslope contributing area as a proxy for hillslope location, and we introduce and test two new metrics: the maximum angle to the skyline and the hazard area, defined as the upslope area with slope >39˚ that reaches a location without passing over a slope of <10˚. We then test the skill with which each metric can identify landslide hazard - the probability of being hit by a landslide - using inventories of landslides triggered by six recent earthquakes. We find that the maximum skyline angle and hazard area provide the most skilful predictions, and these results form the basis for two simple rules: 'minimize your maximum angle to the skyline' and 'avoid steep (>10˚) channels with many steep (>39˚) areas that are upslope'. Because local slope alone is a skilful predictor of landslide hazard, we can formulate a third rule as 'minimise local slope, especially on steep slopes and even at the expense of increasing upslope contributing area, but not at the expense of increasing skyline angle or hazard area'. Upslope contributing area, by contrast, has a weaker and more complex relationship to hazard than the other predictors. Our simple rules complement, but do not replace,

detailed site-specific investigation; they can be used for initial estimation of landslide hazard or guide decision-making in the absence of any other information.

Keywords: coseismic, landslide, heuristic, hazard, exposure

1. Introduction

Landslides involve the downward movement of soil or rock under gravity, sometimes mixing with water or air to run out rapidly over long distances. Landslides have considerable destructive potential and constitute a major hazard to life and infrastructure (e.g. Alexander 2005; Petley, 2012; Klose et al., 2016; Mertens et al., 2016).

Landslide risk can be mitigated by either reducing exposure - the likelihood that a particular person or structure is hit by a landslide - or by reducing the consequences of landslide impact. The latter is expensive for a building (Fell et al. 2005; Volkwein et al., 2011; Guillard-Gonçalves et al., 2016) and extremely difficult for a person (Petley, 2012, Kennedy et al., 2015). As a result, efforts in reducing landslide risk tend to focus on reducing exposure, primarily by siting infrastructure and assets (or choosing to spend time) in places of lower landslide hazard. These choices, however, require information on landslide hazard at a scale that can enable informed decisions about how to respond to that hazard.

Quantitative landslide hazard information is commonly expressed as a relative weighting or probability of landslide occurrence in a given location and over a specified period of time. This is often communicated as a hazard map (Dransch et al., 2010). These maps can provide useful information to inform decisions such as siting infrastructure, allocating resources, designing countermeasures, or planning mitigation measures such as evacuation routes. There are, however, at least five limitations to reliance on hazard maps as the sole source of landslide hazard information. First, landslide hazard maps do not exist for all hazardous locations since their generation requires technical expertise and site-specific information that may not be available. Second, where maps do exist they may not be available to those that need them. Whether in physical or digital form, hazard maps are rarely held by the communities that live within their boundaries (Alexander, 2005; Mills and Curtis, 2008; Twigg et al., 2017). Third, where landslide hazard maps are available their resolution

Nat. Hazards Earth Syst. Sci. Discuss., https://doi.org/10.5194/nhess-2018-271
Manuscript under review for journal Nat. Hazards Earth Syst. Sci.
Discussion started: 13 November 2018

may not be fine enough to address the questions that potential users will have. In everyday decisions, from where to build a house to which way to walk, metres matter for determining landslide exposure. Landslide hazard varies over very short length scales (tens of metres), but national- or even regional-scale hazard maps cannot resolve hazard at those scales, and hazard maps at the appropriate scale would be extremely costly and time-consuming to produce over large areas. Fourth, landslide hazard maps are designed for technical users (such as engineers and planners) and thus can be difficult for non-technical users to interpret (Dransch et al., 2010). Hazard is often expressed in probabilistic terms, which are inherently difficult to communicate and understand (Thompson et al., 2015). The maps may also require particular equipment, such as a computer with appropriate software, or additional contextual information to enable clear visualisation or orient the user (Mills and Curtis, 2008). Finally, landslide hazard maps may lack appropriate information for decision-making. For example, landslide hazard is commonly equated simply with the probability of landslide initiation at a given location, rather than the probability that that location is impacted by a landslide occurring there or somewhere upslope.

In the absence of detailed hazard maps, how should we make decisions about siting infrastructure or spending time in landslide-prone areas? An alternative form of hazard information might be a set of general rules that can be memorised by anyone who might be exposed to landslide hazard, or by those charged with managing landslide risk, to be applied where no other information exists. A good general rule should: 1) be understandable, communicable and memorable; 2) require no prior knowledge, skills or equipment to evaluate; 3) be a skilful discriminant of hazard; and 4) be cast so that it does not increase exposure to another hazard. A good example of such a rule would be the instruction to minimise exposure to tsunami: “in case of earthquake, go to high ground or inland” (Atwater et al., 1999, p20). Research has shown that these types of simple rules are already to some extent implicitly coded into the decisions that people make (e.g. Gigerenzer, 2008), reflecting tacit knowledge of hazards (e.g. Shaw et al., 2008; Lebel, 2013; Twigg et al., 2017). Importantly, however, there are limits to this tacit knowledge (Briggs, 2005); in particular, the body of experience required to generate these rules is limited by both the infrequency of triggering events, such as earthquakes or large storms, and a focus on *normal* rather than *unusual* but not improbable events, introducing biases (McCammon, 2004; Kahneman and Klein, 2009). For example, while perennial rainfall-

triggered landslides and the risks that they pose may be familiar to people in landslide-prone communities, landslides triggered by large earthquakes may fall outside of residents' lived experience, and so will be more challenging to comprehend and account for in decision-making. If simple, memorable rules (fulfilling criteria one and two) could be derived from a large inventory of hazardous events, these biases might be reduced while maintaining the other benefits of a rule-based approach (criteria three and four). Such a set of data-based rules could be used in the absence of, or in conjunction with, existing tools such as hazard maps and local knowledge, both to inform decisions and to inspire discussion amongst householders, local government, and non-governmental organisations. Such knowledge is commonly in demand not only from technical users but from lay people (Twigg et al., 2017; Datta et al., 2018), especially because self-recovery after disasters is increasingly recognised as a critical mechanism of recovery (Twigg et al., 2017).

Here we focus on rules that can be derived from the topography surrounding a given location and that differentiate exposure to coseismic landslide hazard on a scale of tens to hundreds of metres. Such rules are likely to be most useful for decisions before an earthquake about where to site infrastructure or spend time, and may be of less use for decisions during an earthquake when time is limited. We focus on earthquakes because landsliding is an important, but poorly understood, aspect of hazard in many recent continental earthquakes (Huang and Fan, 2013; Roback et al., 2017). Some of our results may be transferrable to landslides caused by more frequent triggers, such as storms, and we consider this point in the discussion.

We examine candidate rules based on our existing understanding of landslide mechanics to identify those that meet criteria one and two above. We then test the skill with which each candidate rule can identify landslide hazard using inventories of coseismic landslides from the recent Finisterre, Northridge, Chichi, Wenchuan, Haiti, and Gorkha earthquakes. Our goal is to determine the rule or rules that best fulfil the four criteria listed above, and that therefore provide the best combination of simplicity and skill in anticipating coseismic landslide impacts. We ask two key questions: (1) to what extent could observed landslide locations have been predicted by these simple rules alone, without recourse to more complex models; and (2) is there a single rule or set of rules that performs well across all earthquakes, and could form the basis for anticipating landslide-affected locations in a future earthquake? While patterns of landsliding in these earthquakes have been previously

established, this is to our knowledge the first attempt to extract a more general set of rules from the combined datasets.

This paper is necessarily technical, addressing the question of whether it is possible to formulate such rules, identifying which rules work best and assessing their performance. We therefore expect the paper's primary audience to be technical experts with an interest in landslide risk reduction. We have begun to explore ways of expressing these rules in a format that is more accessible to a general audience (e.g. Milledge et al., 2018).

2. Potential predictors for coseismic landslide hazard: slope and upslope contributing area

Local slope has been identified as an important driver of landslide occurrence in almost all landslide studies (e.g. Harp et al., 1981; Tibaldi et al., 1995; Keefer, 2000; Wang et al., 2003; Xu et al., 2012, 2013; Parker et al., 2017). This is consistent with mechanistic expectations based on the balance of driving and resisting forces on an inclined failure plane (Taylor, 1937). Local slope is an intuitive parameter that is familiar to most people and can be easily estimated in relative terms (i.e., hillside A is steeper than hillside B) without specialised equipment. Shaking intensity is commonly identified as the other dominant control on coseismic landslide occurrence. However, shaking for any future earthquake cannot be predicted due to lack of certainty on source location, magnitude, rupture style, and local site effects. It is therefore difficult to incorporate into a general rule for future landslide hazard.

Ridges are often considered to be areas of high coseismic landslide probability due to topographic amplification (Densmore and Hovius, 2000), while rivers are by definition areas of flow concentration into which landslides from multiple potential initiation zones may run out. Here we use upslope contributing area as a continuous estimator of the proximity to a ridgeline (defined here as an area with no upslope cells) or a valley, in order to assess how hazard may vary with position in the landscape.

Other predictors have been identified in coseismic landslide studies, but these generally have a secondary effect and are not consistently identified as controls (Parker et al., 2017). Elevation and aspect in particular lack a consistent explanation or pattern as a control on coseismic landslide

hazard (Parker et al., 2017). Other common predictors are difficult to evaluate 'on the ground' without specialised equipment or knowledge. Soil type, rock type, or land cover may be relevant to slope stability but are difficult to identify without specialised training. Curvature is strongly dependent on the length scale over which it is measured and is extremely difficult to estimate by eye, particularly in rough natural topography. Proximity to roads is often possible to estimate in the field, but inclusion of this factor assumes that all roads are similar in their design, age and construction, and thus have similar impacts on slope stability.

3. Accounting for runout in landslide hazard: reach angle and runout routing

All of the potential predictors described above are linked to the probability of coseismic landslide initiation. Once triggered, however, landslide material may run out for long distances and over large areas. Thus, there are substantial portions of any landscape where landslide initiation is unlikely but where contact with a landslide is still possible – for example, at the foot of a steep hillslope. Mechanistic modelling of landslide runout is computationally intensive and strongly sensitive to initial conditions, taking it beyond the capacity of exposed communities (e.g., George and Iverson, 2014). In contrast, simple empirical approaches that have shown some predictive power fall into two categories: reach angles and runout routing.

The Fahrboschung or reach angle from the crown of the landslide to the toe of its deposit has been shown to follow an exponential decrease with landslide volume (Heim, 1882; Corominas, 1996; Hunter and Fell, 2003). The reach angle concept has been incorporated into a small number of hazard maps as a way to represent the probability that a landslide will reach a given location, and can be coupled with predictions of the probability of landslide initiation (e.g. Kritikos et al., 2015). However, these complex combinations of probability are difficult to distil into a single simple rule and to our knowledge, this has not yet been done.

If initiation probability is unknown and we make the conservative assumption that any cell can initiate a landslide, then the hazard at a given location becomes proportional to the area that protrudes above a cone with its apex at the location of interest and its sides inclined at a critical reach angle from the horizontal. This approach has similarities with local sloping base level (Jaboyedoff et al., 2004) and excess topography metrics (Blöthe et al., 2015), which both project surfaces through the

landscape to identify less stable zones, though neither of these approaches are framed in terms of reach angles. Even this simple approach, which neglects initiation probability, is hard to distil: 1) its conceptual complexity makes it difficult to communicate; 2) its predictions depend on a reach angle parameter that is poorly constrained; and 3) the area protruding from an imaginary surface projected beneath the land surface is very difficult to estimate by eye, particularly where significant areas may be occluded from the viewpoint. An alternative metric would simply be the maximum angle from the horizontal to the skyline, which can be interpreted as the maximum (or worst-case) reach angle for that location. This metric is much simpler and thus easier to communicate and remember, can be estimated by eye, and avoids the problem of choosing a critical reach angle.

Runout routing approaches assess the probability that landslide debris will reach a given location by assuming that it flows downslope and that its probability of stopping is dependent on some local property of the path along which it flows. This approach ranges in complexity from detailed physics-based treatments (George and Iverson, 2014; von Ruette et al., 2016) to simple empirical rules such as the local slope or junction angle of flowpaths (Benda and Cundy, 1990; Fannin and Wise, 2001; Montgomery and Dietrich, 1994; Densmore et al., 1998). Hazard estimates are then a function of the initiation probability integrated over the upslope area and the stopping probability for each potential event. To incorporate these considerations as simply as possible, we introduce a new approach (described below) that accounts for local slope at both the locations of landslide initiation and along the flow path. While this approach does not capture the dynamic behaviour of landslide initiation or runout, we include it so that we can test the skill of such non-local approaches and the need to account for them in our simple rules.

4. Earthquake inventories

4.1. 1994 M_w 6.7 Northridge

Topographic relief and seismicity in southern California are associated with dextral transpression at the Pacific-North America plate boundary (Montgomery, 1993). The study area lies within the western Transverse Ranges of southern California and is largely underlain by weakly cemented sedimentary rocks except for the mainly granitic and gneissic San Gabriel and Verdugo mountains and stronger sedimentary rocks in the Simi Hills (Colburn et al., 1981; Tsutsumi and Yeats, 1999;

Parise and Jibson, 2000). Estimated denudation rates for the Santa Monica and San Gabriel mountains are 0.1-1 mm/yr (Meigs et al., 1999; Lave and Burbank, 2004). The region has a warm-summer Mediterranean climate (Peel et al., 2007) with monthly average temperatures ranging from 1 - 18 ˚C (NOAA, 2017) and mean annual precipitation of 0.3–0.9 m (National Atlas of United States, 2011). Vegetation is predominantly annual grassland, sage scrub, and chaparral with some piñon-juniper, oak and pine woodlands (Griffith et al., 2016).

The M_w 6.7 Northridge earthquake occurred on 17 January 1994 and ruptured 14 km of a south dipping (35°) blind thrust fault with a hypocenter at 19 km depth (Wald and Heaton, 1994, Hauksson et al., 1995). The earthquake produced recorded ground accelerations of up to 2 *g* (Harp and Jibson, 1996) and maximum surface displacements of ~4 m. More than 11,000 landslides were triggered across a total area of ~10,000 km^2 (Harp and Jibson, 1996). Landslides were mapped immediately after the earthquake using field studies and aerial reconnaissance and were manually digitized on 1:24,000 scale base maps. Landslides >10 m across could be confidently identified and location errors were estimated to be <30 m (Harp and Jibson, 1996).

4.2. 1993 M_w 6.9 Finisterre

Oblique convergence of the Australian and Pacific plates has driven uplift of the Finisterre Mountains to an elevation of ~4 km since 3.7 Ma (Abbott et al., 1997). The Finisterre Mountains consist of volcanic and volcaniclastic rocks thrust over coarse-grained foreland deposits and capped by limestones (Davies et al., 1987; Abbott et al., 1994). Denudation rates in these mountains are up to 0.3 mm/yr averaged over the time of range formation (Abbott et al., 1997). The region has a tropical climate (Peel et al., 2007), with high and stable monthly average temperatures (26-27˚C) and mean annual precipitation ranging from ~2.5 m in the west to ~4 m in the east (Hovius et al., 1998). The vegetation is predominantly tropical wet or tropical montane evergreen forest with sub-alpine grasslands on some of the higher peaks (MacKinnon 1997; Paijmans 1975).

A M_w 6.9 earthquake occurred on 13 October 1993, with a hypocentre at 25 km depth, rupturing the north-dipping Ramu-Markham thrust fault to within a few hundred meters of the surface (Stevens et al., 1998). The event was followed by multiple aftershocks (5 > M_w 6) including a M_w 6.7 event on 25 October 1993 with a hypocentre at a depth of 30 km. About 4,700 landslides with a total surface area

of about 55 km^2 were triggered by these earthquakes and were mapped from 30 m resolution SPOT images (Meunier et al., 2007).

4.3. 1999 M_w 7.6 Chi-Chi

Taiwan's mountains are the product of oblique collision between the Philippine Sea plate and the Eurasian continental margin. The study area lies within the central mountains of Taiwan and is largely underlain by Neogene sediments and older metasedimentary rocks (Lin et al., 2000). Denudation rates in the central mountains of Taiwan are high, averaging 3-7 mm/yr (Dadson et al., 2003). The region has a humid subtropical climate (Peel et al., 2007) with a mean annual temperature of 22˚C, a mean annual precipitation of 2.5 m and an average of four typhoons per year (Wu and Kuo, 1999). Subtropical moist broadleaf forests occupy most of the island including its mountainous interior (Olsen et al., 2001).

The M_w 7.6 Chi-Chi earthquake occurred on 21 September 1999 with a hypocentre at 8–10 km depth, rupturing ~100 km of the east-dipping Chelungpu thrust fault (Shin and Teng, 2001). The earthquake produced recorded ground accelerations of up to 1 *g* (Lee et al., 2001) and maximum surface displacements of ~8 m (Chi et al., 2001; Shin and Teng, 2001). The earthquake triggered more than 20,000 landslides with the majority occurring across a 3,000 km^2 region (Dadson et al., 2004). Landslides were mapped by the Taiwan National Science and Technology Centre for Disaster Prevention from SPOT satellite images with a resolution of 20 m; landslides with areas >3,600 m^2 were resolved, with location errors estimated to be ~20 m (Dadson et al., 2004).

4.4. 2008 M_w 7.9 Wenchuan

The Longmen Shan mountain range defines the eastern margin of the Tibetan Plateau with displacement taken up mainly on oblique dextral-thrust faults (Burchfiel et al., 1995; Densmore et al., 2007). The Longmen Shan are underlain by a complex lithological assemblage comprising Proterozoic granitic massifs, a Palaeozoic passive margin sequence, a thick Triassic-Eocene foreland basin succession, and minor exposures of poorly-consolidated Cenozoic sediment (Burchfiel et al., 1995). Denudation rates are estimated at ~0.5 mm/yr over decadal to millennial

timescales (Ouimet et al., 2009; Godard et al., 2010; Liu-Zeng et al., 2011). The region has a humid subtropical climate (Peel et al., 2007), with an annual average temperature of 15-17 °C and average annual rainfall varying from ~1100 mm at the margin to ~600 mm on the plateau, of which 70%–80% falls from June to September (Liu-Zeng et al., 2011; Li et al., 2016). The natural vegetation is montane broad-leaved and conifer forest below 4000 m with alpine shrub land and steppe vegetation at higher elevations (Yu et al., 2001).

The M_w 7.9 Wenchuan earthquake occurred on 12 May 2008, rupturing ~320 km of the steeply northwest-dipping Yingxiu-Beichuan and Pengguan faults (Xu et al., 2009). It had an oblique dextral-thrust focal mechanism with a hypocentre at 14-19 km depth. The earthquake produced recorded ground accelerations of up to 1 *g* (Li et al., 2008) and maximum vertical and dextral displacements of 6.2 m and 4.5 m, respectively (Liu-Zeng et al., 2009; Gorum et al., 2011). The earthquake triggered more than 60,000 landslides across a total area of 35,000 km^2 (Gorum et al., 2011; Li et al., 2014). We used a subset of the landslide inventory compiled by Li et al. (2014), who mapped landslides from high-resolution (<15 m) satellite images and air photos. The subset of 18,700 landslides (all mapped landslides east of 104 E), was chosen to avoid gaps in the 30 m resolution SRTM topographic data. Location accuracy for landslides is thought to be similar to the pixel size of the satellite images used, ~15 m (Li et al., 2014).

4.5. 2010 M_w 7.0 Haiti

Haiti's mountains are the product of oblique convergence between the Caribbean and North American plates (Pubellier et al., 2000). The study area is underlain by northwest-southeast oriented sub-parallel belts of igneous, metamorphic and sedimentary rocks (Sen et al., 1988, Escuder-Viruete et al., 2007). Mean elevation and relief generally increase from north to south, to a plateau at ~2500 m (Gorum et al., 2013). The region has a tropical climate (Peel et al., 2007) with a mean annual temperature of 25˚C and mean annual precipitation of ~1.2 m, with two rainy seasons per year (April-June and October-November) and hurricanes between June and November (Gorum et al., 2013; Libohova et al., 2017). The study area lies predominantly within the moist broadleaf forest

biome with some pine or dry broadleaf forest (Olsen et al., 2001) but also has extensive (~50% by area) savannah, shrub or herbaceous cover (Churches et al., 2014).

The M_w 7.0 Haiti earthquake occurred on 12 January 2010, with a hypocentre at 13 km depth but without any detectable surface rupture (Mercier de Lépinay et al., 2011). The complex rupture involved both the Léogâne blind thrust fault, responsible for ~80% of the seismic moment (Hayes et al., 2010) as well as deep lateral slip on the Enriquillo–Plantain Garden Fault (Hayes et al., 2010, Mercier de Lépinay et al., 2011). The earthquake triggered more than 30,000 landslides across a 3,000 km^2 region (Xu et al., 2014). We used an inventory of 23,679 landslides mapped by Harp et al. (2016) from publicly available satellite imagery with a resolution 0.6 m before and after the earthquake; landslides with areas >10 m^2 were resolved (Harp et al., 2017).

4.6. 2015 M_w 7.8 Gorkha

The Himalayas are the product of active continental convergence of India and Asia, much of which is accommodated by the seismogenic Main Himalayan Thrust (Lavé and Avouac, 2000). The study area is underlain by variably metamorphosed sedimentary and igneous rocks of Proterozoic and early Paleozoic age with Paleozoic and Mesozoic sedimentary rocks and low-grade metasedimentary rocks to the north marking the southern margin of the Tibetan Plateau (Hodges et al., 1996; Searle and Godin, 2003; Craddock et al., 2007). Denudation rates in the study area range from 0.3-3 mm/yr over millennial time scales (Lupker et al., 2012; Godard et al., 2014). Mean annual temperature varies with elevation across the study area from ~18˚C in the valley bottoms to -6˚C at high elevations. Average annual rainfall is also topographically controlled, ranging from ~1 m/yr at the range front to >3 m/yr in two bands along the southern margins of the Lesser and Greater Himalaya to <0.5 m/yr on the Tibetan plateau (Bookhagen and Burbank, 2006). Natural vegetation is dominated by temperate broadleaf and coniferous forests up to 3000 m with alpine tundra above the tree line (Singh and Singh, 1987).

The M_w 7.8 Gorkha earthquake occurred on 25 April 2015, rupturing ~140 km of the north-dipping Main Himalayan Thrust (Hayes et al., 2015; Elliott et al., 2016). It had a hypocentre at 8.2 km depth but did not rupture to the surface (Hayes et al., 2015). The event was followed by a series of large

316 aftershocks, including a M_w 7.2 event on 12 May which ruptured a portion of the Main Himalayan
317 Thrust directly east of the 25 April rupture (Avouac et al., 2015). The earthquake triggered
318 approximately 25,000 landslides with a total surface area of about 87 km^2 (Roback et al., 2017). We
319 used an inventory of 24,915 landslides mapped by Roback et al. (2017) from Worldview-2
320 Worldview-3 and Pleiades imagery, with a resolution <0.5 m, before and after the earthquake.
321
322 ## 5. Methods
323 ### 5.1. Conditional probability
324 Landslide hazard can be defined as the probability of being hit by a landslide in a given location
325 and within a given time window (Lee and Jones, 2004). Here we make no distinction between
326 consequences of being hit by landslides of different sizes or velocities, assuming that all are
327 equally dangerous. This probability can be expressed mathematically as P(L|x,y,t), where L is the
328 outcome of being hit by a landslide, *x*,*y* are the coordinates for a particular location and t is the time
329 window of interest. We do not address the timing of landsliding, assuming that this is driven by the
330 timing of an earthquake and is thus unpredictable (Geller, 1997). Instead we focus on landslide
331 susceptibility given an earthquake that produces shaking of unknown intensity at a location (*x,y*),
332 hence the notation P(*L*|*x*,*y*). We assume that the hazard at that location can be approximated by
333 some location-specific characteristic (*a*). Thus, the landslide hazard at (*x,y*) is the conditional
334 probability of being touched by a landslide given the value of the characteristic at that location,
335 P(*L*|*a*), and can be calculated using Bayes Theorem:
336
337 $$P(L|a) = \frac{P(L)\,P(a|L)}{P(a)} \quad (1)$$
338
339 where *a* is a specific characteristic of the location (e.g., the topographic slope). If we assume that
340 the relationships between past landslides and local characteristics are good predictors of their future
341 relationships then we can construct empirical conditional probability calculations from landslide
342 inventories. If we grid the topography, then the Bayes equation can be easily rewritten in terms of

the numbers of grid cells, and in this form the direct equivalence of landslide conditional probability and landslide area density (e.g., Meunier et al., 2007; Dai et al., 2011; Gorum et al., 2014) is clear:

$$P(L|a) = \frac{N(a \cap L)}{N(a)} \quad (2)$$

where N($a \cap L$) is the number of cells with a given value of characteristic *a* that are touched by a mapped landslide, N(*a*) is the number of cells with the characteristic of *a* in the entire study area, and the study area is defined by the smallest convex hull that contains all of the observed landslides. To account for variability in the magnitude of shaking between the six study areas, we normalise the conditional probability of being hit by a landslide P($L|a$) by the study area average probability of landsliding P(*L*) to generate a relative hazard. This can be shown to be directly equivalent to the 'frequency ratio' (e.g., Lee and Pradhan, 2007; Lee and Sambath, 2006; Yilmaz, 2009; Kritikos et al., 2015):

$$\frac{P(L|a)}{P(L)} = \frac{N(a \cap L) / N(a)}{N(L) / N(S)} = \frac{N(a \cap L)}{N(a)} \frac{N(S)}{N(L)} \quad (3)$$

where N(*S*) is the total number of cells in the study area and N(*L*) is the number of cells touched by landslides. Our normalised conditional probability is also directly equivalent to the 'probability ratio' used by Lin et al. (2008) and Meunier et al. (2008) since, from Bayes Theorem:

$$\frac{P(L|a)}{P(L)} = \frac{P(L)\,P(a|L)}{P(a)P(L)} = \frac{P(a|L)}{P(a)} \quad (4)$$

We display the normalised conditional probability on a logarithmic scale for readability, resulting in a probability metric that is strongly similar to the 'information value' metric used in some landslide susceptibility analyses (e.g., Yin and Yan, 1988).

Conditional probability analysis is advantageous for its direct link to hazard and does not require us to impose a functional form to the data. However, the results are partly dependent on bin size and

location for the predictor variable, and bins with few observations (i.e. N(*a*)<<N(*S*)) can result in noisy data that are difficult to interpret. To aid interpretation in the presence of noise, we fit cubic polynomial functions to one-dimensional conditional probability data and a logistic function to two-dimensional data. To highlight the parts of the data where we have few observations and thus where our confidence in the results is lower, in the one-dimensional case we include a single bulk PDF of the predictor variable on the x-axis below the conditional probability curve, and we limit ourselves to calculating probability only where there are more than 10 observations per bin in the two-dimensional case. Whilst other statistical approaches could be used here (e.g. Pradhan, 2013), our intention is not to find the statistical approach that provides the most powerful synthesis of the different variables, but to test the effectiveness of the variables themselves at distinguishing hazard when applied in the form of simple rules.

5.2. Receiver operating characteristic curves

Any simple rule for identifying more or less hazardous locations in the landscape will produce a relative measure of landslide probability. To evaluate this measure against a binary landslide map or inventory (where every cell is classified as landslide or non-landslide), it must be converted into a binary classification. A common approach to this problem is to construct a receiver operating characteristic (ROC) curve (e.g., Frattini et al., 2010). This curve quantifies both the benefit of a given classification in terms of successfully classified outcomes (landslide and non-landslide locations correctly identified, true positives and true negatives respectively) and also the cost (non-landslides identified as landslides, false positives; and vice versa, false negatives). The ROC curve is constructed by thresholding a continuous variable (e.g., slope) and calculating the true positive rate as the number of true positives normalised by all positive observations, and the false positive rate as the number of false positives normalised by all negative observations. Evaluation of these rates at different threshold values results in a curve, where the 1:1 line reflects the naïve (i.e. random) case. The area under the curve (AUC) tends to 1 as the skill of the classifier improves towards perfect classification and to 0.5 as the classifier worsens towards the naïve (random) case. We calculate ROC curves for all of our chosen predictive approaches for each inventory.

399 ### 5.3. Topographic analysis

400 All of the metrics tested here are defined using topographic data in the form of digital elevation
401 models (DEMs). We use 30 m resolution DEM data at all sites: for Northridge they are derived from
402 the down-sampled 10 m NED elevation data (https://lta.cr.usgs.gov/NED), while for all other sites we
403 use 1-arc sec Shuttle Radar Topography Mission (STRM) elevation data (http://srtm.csi.cgiar.org/).
404
405 #### *5.3.1. Slope and upslope contributing area*

406 We calculate local slope as the steepest path to a downslope neighbour from each cell (Travis et al.,
407 1975) because calculating slope over larger (e.g. 3x3 cell) windows for a 30 m resolution DEM results
408 in considerable underestimation (Claessens et al., 2005). We calculate upslope contributing area
409 using a multiple flow direction algorithm (Quinn et al., 1991) having filled pits using a flood fill
410 algorithm (Schwanghart and Kuhn, 2010). These topographic analyses are performed in Matlab
411 using TopoToolbox v1.06 (Schwanghart and Kuhn, 2010).
412
413 #### *5.3.2. Skyline angle analysis*

414 To capture the effect of both initiation and runout we define the skyline angle as the maximum angle
415 from horizontal to the skyline for a given location. This is easily estimated by eye in the field and can
416 be interpreted as the maximum (or worst-case) reach angle for that location. It is a runout-dominated
417 metric in that it does not take into account the probability of initiation.
418 For each cell in a study area we estimate the skyline angle by calculating vertical angles between
419 the target cell and every other cell within a 4.5 km radius. This radius is chosen to exceed the
420 dominant channel spacing for the study area with widest spacing (Wenchuan) and thus to fully
421 capture the local skyline. For the Wenchuan study area the characteristic hillslope length, estimated
422 following the method of Roering et al. (2007), is ~500 m. Thus a conservative estimate on dominant
423 channel spacing would be ~1 km. We choose larger window size because skyline angle estimates
424 become asymptotically insensitive to window size, so that the only constraint is run time. MATLAB
425 code for the routine is included in the supplemental information. This approach is physically limited
426 in at least two ways (Figure 1a). First, it does not account for the dependence of runout on the size
427 of the initial failure or how the failure volume may increase or decrease during runout (e.g.

Nat. Hazards Earth Syst. Sci. Discuss., https://doi.org/10.5194/nhess-2018-271
Manuscript under review for journal Nat. Hazards Earth Syst. Sci.
Discussion started: 13 November 2018

428 Corominas, 1996). Second, it does not honour flow paths. The skyline cell that generates the
429 steepest slope to the target cell does not have to be connected to the target cell by a flowpath with
430 monotonically decreasing elevation. However, this metric provides a measure of the gravitational
431 potential energy available to drive runout in the vicinity of the target cell.

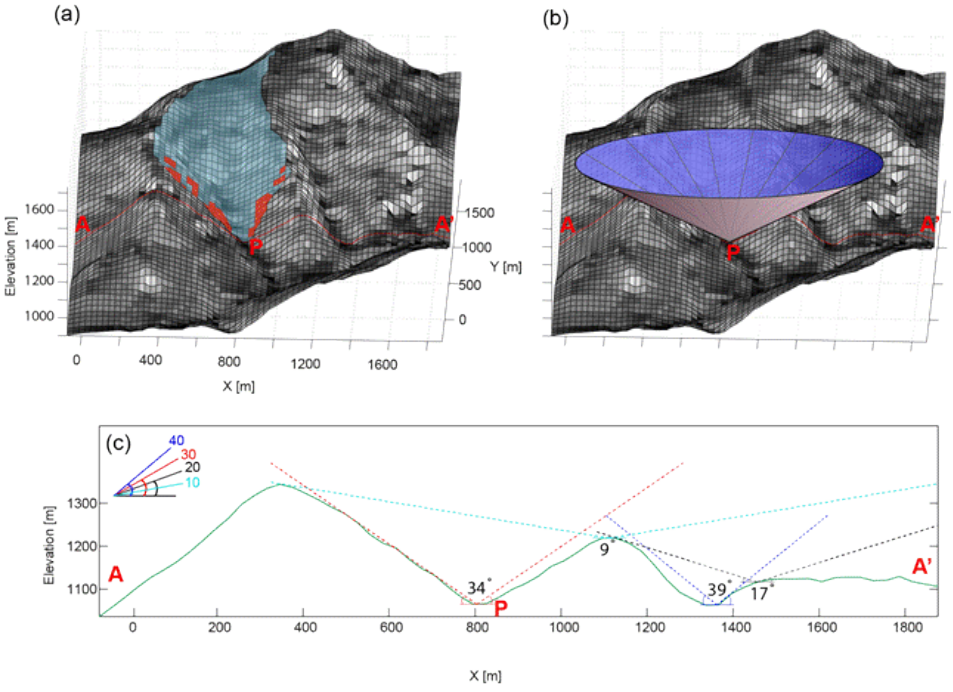

432

433 **Figure 1.** Schematic view of the different topographic metrics tested here. (a), perspective view of a
434 landscape with each cell shaded according to its local slope from light (steep) to dark (gentle). The
435 upslope contributing area for point P is coloured blue, and the cells steeper than 39˚ that have a flow
436 path to P that is never less than 10˚ are coloured red. (b), the same perspective view with a cone
437 projected from point A at an angle of 34˚ so that the surface of the cone is in places tangent to but
438 never intersects the ground surface, indicating a maximum skyline angle of 34˚ for point P. (c), cross
439 section A-A' through the landscape (highlighted in red on panels a and b) with dashed lines showing
440 skyline angles at four example locations.

441

442 **5.3.3. Runout routing analysis**

443 To assess the importance of non-local runout paths on landslide probability, we follow the approach
444 of Dietrich and Sitar (1997) who proposed the simplest possible debris flow runout model, requiring

only thresholds to define instability and for downslope motion to continue. This simple model, referred to as SHALRUN, was integrated with the coupled hydrologic-slope stability model SHALSTAB in an efficient parallel framework to predict landslide hazard potential in California (Bellugi et al, 2011). SHALRUN required only two field-calibrated parameters: a critical rainfall threshold to define instability, and a minimum slope threshold for downslope motion to continue. To apply this model in the context of coseismic landslides (SHALRUN-EQ) we modify the condition for landslide initiation, replacing the critical rainfall threshold with a slope threshold. We thus assume that landslide initiation and deposition are entirely dependent on the local slope of the ground surface θ (i.e., landslides are more likely to initiate on steeper slopes and deposit on flatter slopes), further increasing the simplicity of the model. More formally, SHALRUN-EQ predicts the upslope hazard area A_h as the upslope area weighted by the joint probability of landslide initiation and runout. Locations with higher A_h should have higher exposure to coseismic landslide hazard than those with low (or no) A_h. Formulation of the model requires: (1) determination of the mobilisation probability at each cell i in the study area (P_{mi}); (2) determination of the connection probability for mobilised material from each cell i to the target cell j (P_{cij}); (3) convolution of (1) and (2) to get the locational hazard (P_{mcij}); and (4) accumulation of the locational hazard to determine a hazard area above each target cell j (A_{hj}).

In order to generate a simple rule, our model assumes that landslide initiation and deposition are entirely dependent on the local slope of the ground surface θ (i.e. landslides are more likely to initiate on steeper slopes and deposit on flatter slopes). For landslide initiation, we assume that slopes above a threshold slope θ_m are all equally capable of initiating a landslide with probability P_{mi}:

$$P_{mi} = \begin{cases} 1 : \theta_i \geq \theta_m \\ 0 : \theta_i < \theta_m \end{cases} \quad (5)$$

where θ_i is the observed local slope in a downslope direction at cell i and θ_m is the critical slope required for landslide initiation.

In order to represent a landslide hazard, mobilised material must be able to runout from the initiation point to the target cell j. This relationship is binary: either these points are connected by a viable

runout path or they are not. We assume that the flow path will follow the path of steepest descent. This path must enable continued runout for its entire length; if at any point on the flow path the material is fully deposited, then that initiation zone will be disconnected from cell j. Thus, the point along a given flow path that is most likely to cause deposition becomes the controlling location for the connection of all upslope points. Surface slope has been used to describe the probability that landslide material entering a cell will be deposited rather than continuing into the next downslope cell (e.g., Benda and Cundy, 1990; Fannin and Wise, 2001). For landslide deposition, we apply the simplest possible stopping condition, and assume that landslide run-out ceases on slopes gentler than a critical angle (θ_s). The probability that a landslide initiated at point i reaches point j (P_{cij}) can thus be expressed as:

$$Pc_{ij} = \begin{cases} 1: \theta min_{ij} \geq \theta_s \\ 0: \theta min_{ij} < \theta_s \end{cases} \quad (6)$$

where θmin_{ij} is the minimum slope for the flow path from cell i to cell j, and θ_s is the critical slope required for stopping.

We combine the initiation and runout probabilities to calculate the locational hazard P_{mcij} as the area (a_i) in cell i weighted by the probability that a landslide is both mobilised in cell i and is connected to cell j:

$$P_{mcij} = a_i \, P_{mi} \; P_{cij} \quad (7)$$

Assuming that $\theta_s > 0$, we calculate the hazard area A_{hj} for each target cell j by summing locational hazard in the n cells upslope of j, normalised by the unit contour length to minimise grid resolution bias:

$$A_{hj} = \sum_{i=1}^{n} \left(\frac{a_i}{l_j} \, P_{mi} \; P_{cij} \right) \quad (8)$$

where l_j is the unit contour length at j, calculated as $a_j^{0.5}$. Equation 8 is evaluated for every cell in the study area to generate a spatial grid of hazard area A_h (Figure 2). Our choice of step functions for the mobilisation (P_m) and connection (P_c) probabilities allows us to interpret A_h as the upslope area per unit contour width with local slope steeper than θ_m from which a landslide will reach the cell of interest by moving downslope along a path that is always steeper than θ_s. Alternative formulations could be used for P_m and P_c but these would result in a less intuitive index that would be difficult to implement as a simple rule.

There is implicit resolution dependence to the stopping condition θ_s since it assumes that the low gradient area is long enough (in terms of flow path length) that the landslide will stop. Similarly, there is resolution dependence to the initiating condition θ_m as topographic surfaces will be more or less smooth, depending on the resolution of the DEM (Classens et al., 2005). Also, the initiation probability is based on local slope alone and so does not account for any of the other possible drivers of coseismic landslide initiation, such as topographic amplification (Meunier et al., 2008), or pore water pressure (e.g., Xu et al., 2012). While many more complex models exist that account for initiation volumes and flow dynamics (e.g., George and Iverson, 2014; von Ruette et al., 2016), we seek the simplest possible model that captures the effects of drainage networks in accumulating hazard, of steep slopes in landslide initiation, and of gentle slopes in landslide deposition.

The model has two parameters (θ_m and θ_s), both of which are effective rather than measurable. We first optimise the model for each inventory to establish its performance under the best possible scenario, where the model is fitted to the data. We then test the model using the average of the optimised parameters from the six inventories to represent a more realistic application where these parameters must be estimated from previous events. Thus, the values of θ_m and θ_s should not be interpreted as mechanistic thresholds, but rather as the result of an optimization that also depends on the DEM resolution.

Nat. Hazards Earth Syst. Sci. Discuss., https://doi.org/10.5194/nhess-2018-271
Manuscript under review for journal Nat. Hazards Earth Syst. Sci.
Discussion started: 13 November 2018

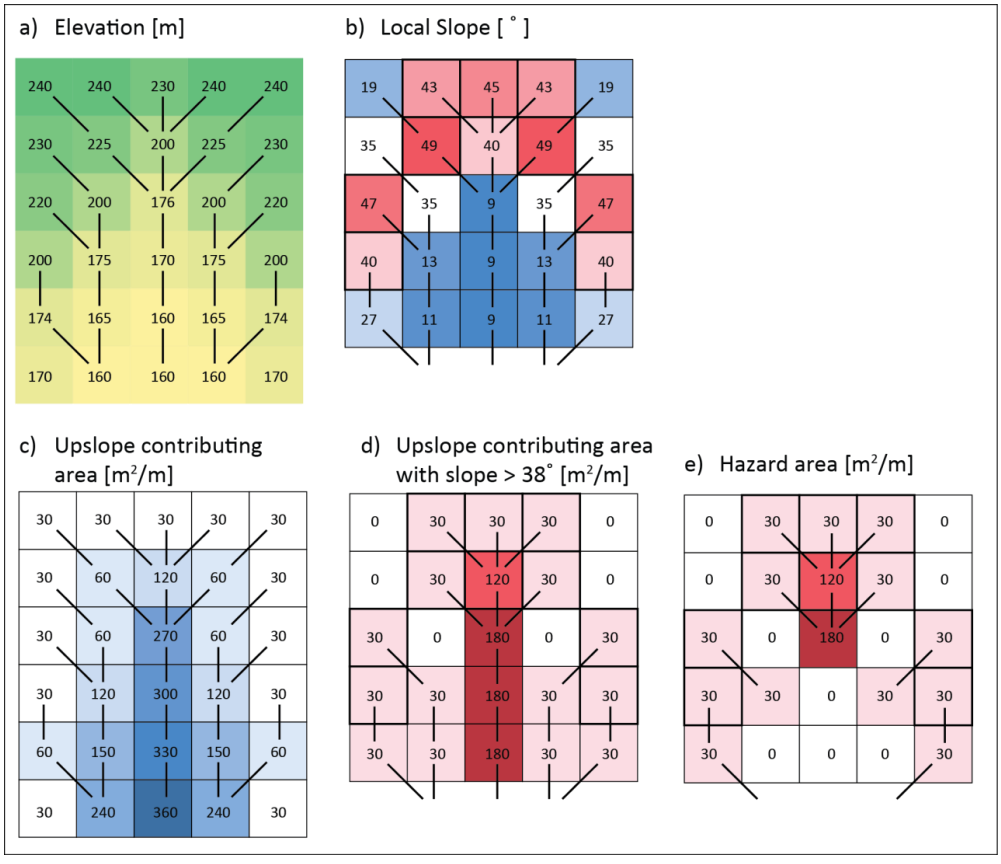

Figure 2. Worked example of SHALRUN-EQ hazard area calculations for an initiation angle of 39° and a stopping angle of 10°. a), elevations from a 30 m resolution digital elevation model for an area of topographic convergence. Lines show steepest flowpaths from cell to cell. b), local slope calculated as the steepest path to a downslope neighbour. Thick outlines show cells steeper than 38°. c), upslope contributing area using steepest flow path routing. d), upslope contributing area steeper than 38°. e), hazard area, defined as the upslope area steeper than 38° with flow paths that do not fall below 10°.

Nat. Hazards Earth Syst. Sci. Discuss., https://doi.org/10.5194/nhess-2018-271
Manuscript under review for journal Nat. Hazards Earth Syst. Sci.
Discussion started: 13 November 2018

6. Results

6.1. Local slope

For all inventories, landslide probability increases as an approximately exponential function of local slope (Figure 3a). For four of the six inventories, conditional probability exceeds the study area average probability for slopes steeper than 30-35˚, with Northridge and Haiti lower at 20˚ and 25˚. This suggests that slopes <30˚ are generally safer than average, while those >45˚ have a landslide probability >200% of the average, and those >50˚ are generally >300% of the average. The curves for Finisterre, Chi-Chi and Gorkha largely collapse on each other when normalised by study-area average probability (Figure 3a). However, landslide hazard is less sensitive to slope for Wenchuan and more sensitive for Northridge and Haiti. This variability between inventories likely reflects specific study area properties such as the more dissected topography within the Northridge and Haiti study areas. Comparing the amalgamated PDF of study area slopes (Figure 3a) with the conditional probability curves indicates that the majority of the landslide hazard burden is held by the minority of each study area (slopes >35˚). This implies that 1) many of the modest (<15˚) slopes on which people generally choose to live are exposed to relatively low hazard (less than half the study area average for all but Wenchuan); and 2) any choice to spend time or build infrastructure on steeper slopes should recognise the considerable associated increase in exposure to coseismic landslide hazard.

6.2. Upslope contributing area

For all inventories, landslide probability increases from below the study area average at the lowest upslope contributing areas – that is, ridge tops – to a peak or plateau at intermediate upslope contributing areas, from which it declines in four of the six inventories (Figure 3b). Locations with the lowest upslope contributing area also have the lowest landslide probability for four of the six inventories, with Northridge and Finisterre as exceptions. For Northridge, the zone of lower than average landslide probability extends only to upslope contributing areas ~40 m^2/m; for Finisterre it extends to ~100 m^2/m, for Chi-Chi and Haiti to ~150 m^2/m and for Wenchuan and Nepal to ~200 m^2/m. The location of peak landslide probability broadly coincides with the inflection in average slope for a given upslope contributing area (Figure 4). This inflexion is commonly used as an indicator of the transition from hillslopes to rivers (Montgomery and Foufoula-Georgiou, 1993; Stock and

Nat. Hazards Earth Syst. Sci. Discuss., https://doi.org/10.5194/nhess-2018-271
Manuscript under review for journal Nat. Hazards Earth Syst. Sci.
Discussion started: 13 November 2018

563 Dietrich, 2006; Hancock and Evans, 2006), suggesting that maximum (or near maximum) landslide
564 probability occurs at the transition from hillslopes to channels (Figure 3b). Landslide probability
565 decreases with increasing upslope contributing area beyond this transition point for four of the six
566 inventories, gently for Finisterre and Chi-Chi, more steeply for Northridge and Haiti, and in all cases
567 with an increase in scatter that is likely due to the small number of observations with upslope
568 contributing area >1000 m^2/m.

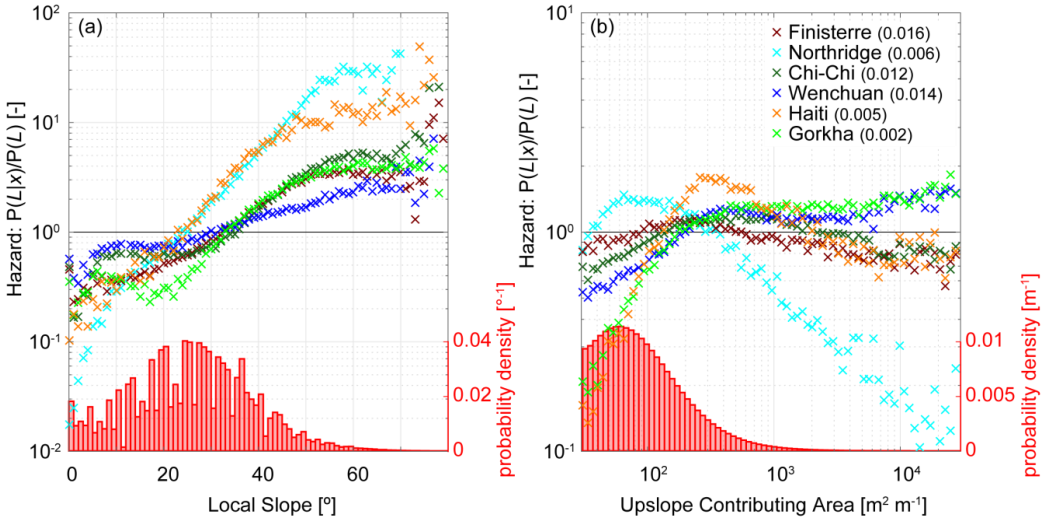

569

570 **Figure 3.** Landslide hazard defined as conditional probability P(*L*|*x*) normalised by study area
571 average landslide probability P(*L*), where *x* is a) local slope and b) upslope contributing area per unit
572 contour length. Red bars show histograms of each variable over the six inventories. Note logarithmic
573 y-axes and different y-axis scales in panels a and b. The solid black lines show a normalised
574 probability of 1, equivalent to the study area average; thus, points above the solid black line have
575 conditional probability greater than the study area average. Legend includes study area average
576 landslide probabilities for each inventory (in brackets).

577

578 **6.3. Local slope and upslope contributing area combined**

579 When slope and upslope contributing area are examined in combination, the highest landslide
580 probability is consistently found at the highest upslope contributing area for a given slope or the
581 highest slope for a given upslope contributing area (Figure 4). The lowest probabilities are found at
582 locations with both low slope and upslope contributing area, and cells with very low slopes have low

583 landslide probability almost independently of upslope contributing area. Importantly, landslide
584 probability increases more steeply with increasing slope than with increasing upslope contributing
585 area, indicating the dominance of local slope in setting landslide probability. This dominance is also
586 reflected in the orientation of the probability contours derived from logistic regression. There is
587 variability in contour orientations between inventories, with Finisterre and Northridge showing the
588 strongest slope dependence and Wenchuan showing the strongest upslope contributing area
589 dependence (Figure 4).
590
591 The shape of the two-dimensional probability surface determines the best course of action in terms
592 of choosing alternative locations for a particular asset or activity, but such action is also constrained
593 by what is possible. The average slope for each upslope contributing area (dashed line in Figure 4)
594 indicates that for Northridge, Finisterre, Chichi and Haiti there are rarely situations where a reduction
595 in upslope contributing area will not involve (on average) an increase in slope, that will actually
596 increase landslide probability. However, for locations in Wenchuan and Gorkha with upslope
597 contributing area of 300 to 10,000 m^2/m, the probability reduction due to reducing upslope
598 contributing area is not offset by the associated increase in slope. This suggests that, for the former
599 inventories, it is always beneficial to decrease slope even at the expense of upslope contributing
600 area, while for the latter it is more dependent on initial location. In general, the average slope contour
601 appears to separate higher and lower than average landslide probability in slope-upslope
602 contributing area space, suggesting that higher than average landslide probability is always found
603 on higher than average slopes for a given upslope contributing area.
604

Nat. Hazards Earth Syst. Sci. Discuss., https://doi.org/10.5194/nhess-2018-271
Manuscript under review for journal Nat. Hazards Earth Syst. Sci.
Discussion started: 13 November 2018

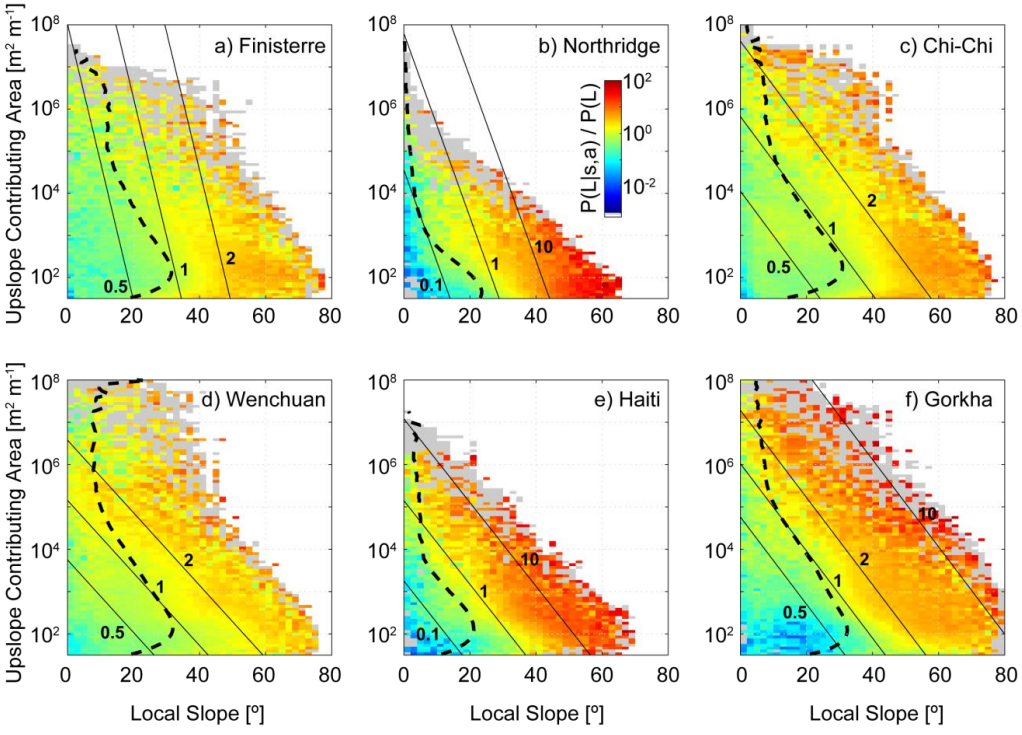

Figure 4. Two-dimensional plots of landslide hazard, defined as conditional landslide probability P(*L*|*s*,*a*) normalised by study area average landslide probability P(*L*), where s is local slope and a is upslope contributing area per unit contour length. Dashed lines show the mean slope per upslope contributing area bin using 100 logarithmically-spaced bins. Solid lines are relative hazard contours from logistic regression in the same units as the relative hazard surface. Grey cells indicate slope-area pairs with data but with no cells touching a landslide. Note that upslope contributing area is shown on a logarithmic axis, so that maintaining a constant landslide probability for a given increase in slope requires a larger reduction in upslope contributing area at low slopes than at high slopes.

615 **6.4. Skyline angle**

616 Landslide probability increases as an approximately exponential function of maximum skyline angle
617 (Figure 5a) as it does for local slope (Figure 3a). Landslide probability exceeds the study area
618 average probability at skyline angles of 27-28˚ for Northridge and Haiti, 34˚ for Wenchuan and 38-
619 40˚ for Finisterre, Chi-Chi and Gorkha. Locations with skyline angles of <20˚ have less than half the
620 study area average landslide probability for all inventories, while those with skyline angles of >50˚
621 have more than double the study area average probability (Figure 5a). The lowest landslide
622 probability values, at skyline angles of less than 10˚, are lower than those for local slope or upslope
623 contributing area. As with local slope, the curves for several of the inventories (Finisterre, Chi-Chi
624 and Wenchuan) collapse to a similar relationship when normalised by study area average probability
625 suggesting similar behaviour across a range of different landscapes. However, Northrige and Haiti
626 show stronger sensitivity to skyline angle and Gorkha shows considerably reduced landslide
627 probability at low skyline angles relative to the other inventories.
628
629 **6.5. Hazard area**

630 The ability of hazard area A_h to distinguish landslide from non-landslide cells is highly sensitive to
631 two tuneable parameters (θ_m and θ_s) but follows a smooth optimisation surface with a unique
632 optimum for each inventory (Figure S1). Optimum parameters vary between inventories, with
633 optimum initiation slopes θ_m ranging from 36˚ to 40˚ and stopping slopes θ_s from 6˚ to 31˚ (Table S1).
634 Since these optimum parameters vary between inventories and can only be identified after an
635 earthquake, they are problematic in terms of incorporation into a rule. Instead, we use the global
636 average of the optimised parameter values from the six inventories (θ_m = 39˚ and θ_s 10˚). The
637 stopping angle of 10˚ is steeper than many, though not all, of the observed slopes on which debris
638 flows stop. For example, Stock and Dietrich (2003) report that debris-flow generally exhibit stopping
639 angles of 2-6˚, but may halt at much larger angles (13-22˚) on open slopes. The steeper angles
640 reported here, may reflect differences in the method and resolution of slope calculation but likely
641 result from the coseismic trigger which does not necessitate high levels of saturation in the initial
642 failure. Conditional probabilities are very low for cells with A_h = 0 (i.e., where no cells steeper than

Nat. Hazards Earth Syst. Sci. Discuss., https://doi.org/10.5194/nhess-2018-271
Manuscript under review for journal Nat. Hazards Earth Syst. Sci.
Discussion started: 13 November 2018

Natural Hazards and Earth System Sciences
Discussions

643 the initiation angle runout over flowpaths steeper than the stopping angle), ranging from 2% to 15%
644 of the study area average (Figure 5b). Conditional probability increases with A_h for all inventories but
645 only slowly for A_h < 1 m^2/m; the trend then steepens to a peak (Northridge, Haiti, Nepal) or plateau
646 (Finisterre, Chichi, Wenchuan) at A_h values of 100 to 1000 m^2/m with conditional probabilities 200 -
647 800% of the study area average (Figure 5b).

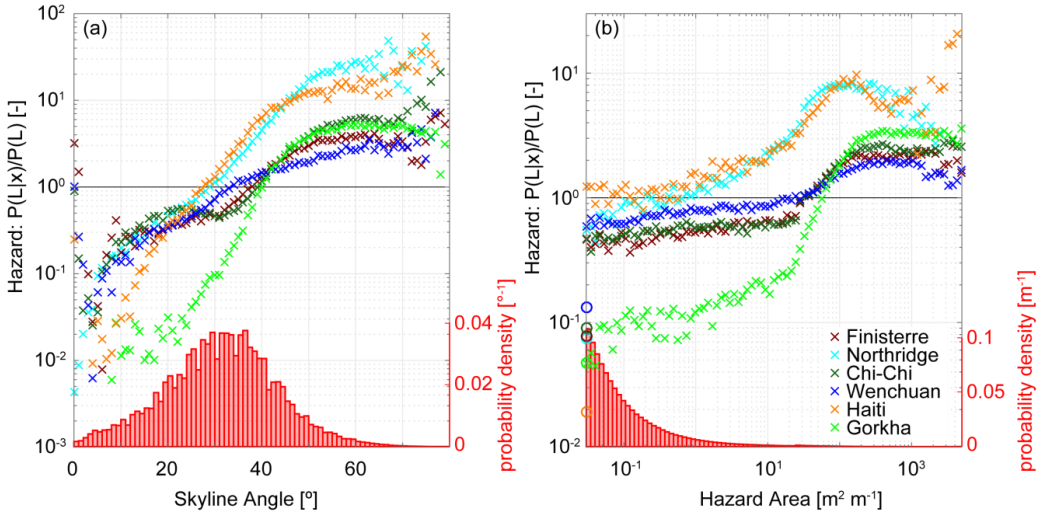

648

649 **Figure 5.** Landslide hazard defined as conditional landslide probability P(*L*|*x*) normalised by study
650 area average landslide probability P(*L*), for a) skyline angle; and b) hazard area with average
651 parameters - that is, the areas with slope greater than 39˚ that have a flow path to the cell of interest
652 and do not travel across a cell with a slope less than 10˚. Red bars show histograms of each variable
653 over the six inventories. Coloured circles on the y-axis in (b) indicate conditional probabilities for cells
654 with a hazard area of 0 m^2/m. Note logarithmic y-axes and different y-axis scales in panels a and b.
655 The solid black lines show a normalised probability of 1, equivalent to the study area average; thus,
656 points above the solid black line have conditional probability greater than the study area average.

657

658 **6.6. ROC analysis**

659 To supplement conditional probability analysis, we examine the performance of slope, upslope
660 contributing area, skyline angle, and hazard area as continuous hazard indices (with high index
661 values reflecting high hazard and vice versa) using ROC curves (Figure 6). Successful indices will
662 capture landslide cells within high hazard index zones (true positives) without capturing non-

landslide cells in the same zones (false positives). Hazard area performs best for all six inventories with an AUC always above 0.78 and an average AUC of 0.83 (Table 1). Skyline angle performs joint best for Haiti and second best for a further three of the six inventories, with AUC always above 0.65 and an average AUC of 0.77. The exceptions, where slope, upslope area, or their combination performs second best are Northridge and Wenchuan. For Northridge slope alone and slope plus upslope contributing area both outperform skyline angle by a single percentage point, while upslope contributing area by itself performs considerably worse (Figure 6a). For Wenchuan, upslope contributing area considerably outperforms the other indices, perhaps reflecting longer-runout landslides in this inventory, while slope performs particularly poorly (Figure 6d). Although slope, upslope contributing area, and their combination all perform better than skyline angle in one of the inventories. none do so consistently across multiple inventories. This is reflected in their averaged AUC values over all inventories of 0.72, 0.72 and 0.73 for slope, upslope contributing area, and their combination respectively.

Table 1. Area under the ROC curve for the five hazard metrics over the six coseismic landslide inventories. The best performing metric for each inventory is in bold, the second best is in italics.

	Hazard area	Skyline angle	Slope + upslope contributing area	Local slope	Upslope contributing area
Finisterre	**0.79**	*0.72*	0.69	0.69	0.66
Northridge	**0.89**	0.83	*0.84*	*0.84*	0.62
Chi-Chi	**0.80**	*0.73*	0.68	0.67	0.69
Wenchuan	**0.78**	0.65	0.62	0.58	*0.74*
Haiti	**0.86**	*0.85*	0.83	0.79	0.69
Gorkha	**0.88**	*0.85*	0.77	0.73	0.76
Average	0.83	0.77	0.74	0.72	0.69
1σ	0.05	0.08	0.09	0.09	0.05

Nat. Hazards Earth Syst. Sci. Discuss., https://doi.org/10.5194/nhess-2018-271
Manuscript under review for journal Nat. Hazards Earth Syst. Sci.
Discussion started: 13 November 2018

Natural Hazards and Earth System Sciences
Discussions

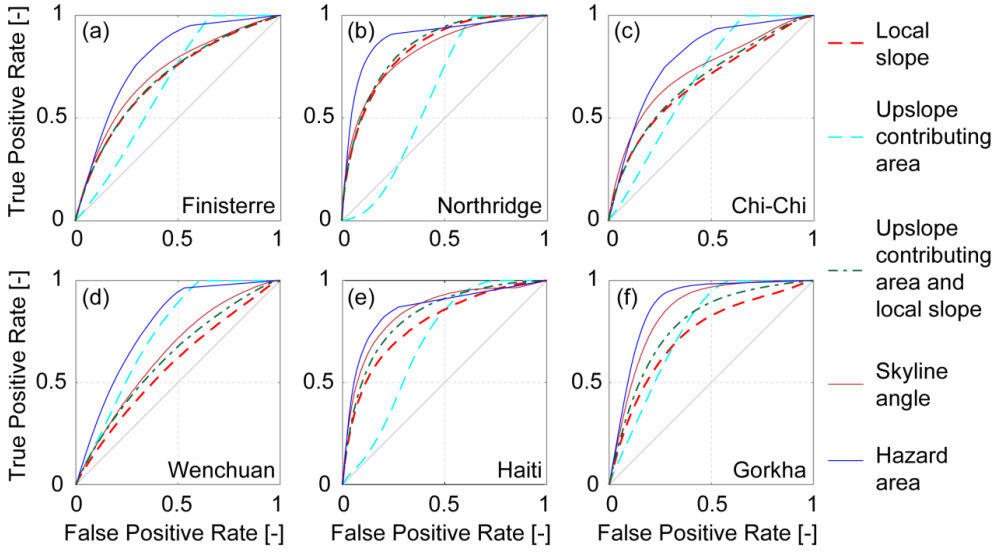

Figure 6. Receiver operating characteristic (ROC) curves for the six inventories: a) Finisterre, b) Northridge, c) Chi-Chi, d) Wenchuan, e) Haiti, f) Gorkha. False positive rate is given by the number of false positives divided by the sum of false positives and true negatives. True positive rate is given by the number of true positives divided by the sum of true positives and false negatives. The 1:1 line represents the naïve (random) case. Curves plotting closer to the top left corner of each panel represent better model performance.

7. Discussion

We structure the discussion around three simple rules that are drawn from the results above. In each case we explain the evidence on which the message is based, why it works, our degree of confidence, and implications for applying the rule. Finally, we examine the spatial implications of these rules using an example landscape.

7.1. Rule 1: avoid steep (>10˚) channels with many steep (>39˚) areas that are upslope

The hazard area is the best or joint best predictor of landslide probability for all six inventories. The hazard area defined by the average initiation angle (39°) and stopping angle (10°) across all six inventories performs nearly as well as the optimised area for each inventory, enabling us to define a

699 general rule independent of any specific inventory. This is fortunate, as site-specific optimisation
700 requires a pre-existing landslide inventory for any individual area and so may not be feasible. In all
701 six inventories, locations with A_h > 60 m^2/m have landslide probability above the study area average.
702 While landslide probability generally increases with increasing hazard area, the relationship is
703 complex (Figure 6). Landslide hazard can be most effectively decreased by decreasing A_h at
704 intermediate values of A_h, whereas decreasing A_h at either the upper or lower extremes has minimal
705 effect on hazard. The qualitative statement to avoid areas with 'many' steep slopes could also be
706 phrased 'any' steep slopes since the landslide probability is generally 5-10 times higher even for
707 very small values of A_h (c. 0.1 m^2/m) than the landslide probability for areas with no A_h.
708 Landslides do not always obey steepest flow path routing rules, and it is possible for landslides to
709 travel up reverse slopes or along contours. This is particularly true for large deep-seated landslides
710 or rockfalls. The hazard area metric cannot account for such behaviour and thus is more likely to
711 reflect hazard from smaller shallow landslides, while skyline angle, which does allow for runout over
712 reverse slopes, may be a better predictor for larger deep-seated landslides. The two indices have
713 some overlap but could be used in combination to find safer locations in the landscape.
714

715 **7.2. Minimise your maximum angle to the skyline**

716 The maximum skyline angle is the second-best predictor of landslide probability in four of the six
717 cases. Locations with skyline angles less than 30˚ generally have a landslide probability below the
718 study area average. Importantly, landslide probability increases non-linearly with skyline angle, so
719 that a slight reduction to a high skyline angle results in a much larger reduction in landslide probability
720 than it would for a lower skyline angle.
721 The distinction between local slope and skyline angle reflects the importance of runout as well as
722 initiation in defining landslide hazard. Landslide hazard is an inherently non-local problem, defined
723 by both conditions at the point of interest and those upslope of that point. The skyline angle is a
724 simple way to represent this. It has the additional advantage of being easy to measure, needing only
725 a protractor or clinometer for precise measurement in the field, and being easily approximated by
726 eye. Local slope, in contrast, is scale-dependent, while upslope contributing area and A_h are both
727 considerably more difficult to estimate in the field.

728

729 **7.3. Minimise local slope, especially on steep slopes, and even at the expense of**
730 **increasing upslope contributing area, but not at the expense of increasing skyline**
731 **angle or hazard area**

732 Local slope generally performs less well than skyline angle or hazard area but is a consistently skilful
733 predictor of coseismic landslide hazard, and could be a useful additional discriminant for situations
734 where both skyline angle and hazard area are comparable between two locations. In this situation,
735 our results suggest choosing the location with the lower local slope. This is particularly true at steeper
736 slopes since landslide probability increases exponentially with slope, approximately doubling for
737 every 10˚ increase in slope.

738 Given the common observation that coseismic landslides initiate near ridge crests (Densmore and
739 Hovius, 2000; Meunier et al., 2007), it is perhaps surprising that landslide hazard generally increases
740 with increasing upslope contributing area (i.e. moving downslope from ridge crests). In fact, while
741 coseismic landslides may initiate preferentially near the ridges, they runout downslope; thus, areas
742 near ridges are less likely to be touched by any part of a landslide even though they are more likely
743 than other parts of the landscape to contain a landslide crest. Landslide probability is consistently
744 low at very low values of upslope contributing area, corresponding to ridges; for some inventories, it
745 is also low at very high values of upslope contributing area, corresponding to valley floors in the
746 downstream reaches of the river network. This may be partly a function of the covariance between
747 local slope and area, since locations with large upslope contributing areas generally have lower
748 slopes (see dashed lines in Figure 4). The addition of upslope contributing area as a predictor in
749 logistic regression improves landslide probability prediction relative to slope alone (Table 1), but the
750 orientation of the probability contours (Figure 4) indicates that its influence is weak. Moving to a
751 location with lower slope angle almost always reduces landslide probability independently of the
752 upslope contributing area of the new location, although the specific reduction of landslide probability
753 depends on the shape of the two-dimensional probability surface (Figure 4). We conclude that
754 decisions on how to reduce landslide hazard most effectively need to be made on a case by case
755 basis, and are best made using hazard area, skyline angle, and the local slope in conjunction with
756 each other. Steep upslope areas result in elevated hazard but gentle upslope areas do not,

757 explaining the improved performance of hazard area relative to upslope contributing area (Figure 6
758 and Table 1). Ridges, with very low upslope contributing area, are generally low hazard locations if
759 they have gentle local slope but can still be hazardous if they are steep (Figure 4). To minimise
760 landslide hazard, it is thus preferable to seek broad ridges over sharp ridges where such a choice is
761 possible.
762
763 **7.4. Movement rules in a landscape with variable hazard**
764 While this analysis is focused on cell-by-cell hazard assessment, and is thus appropriate for
765 decision-making before a large earthquake, it is also possible to use the results to define some rules
766 for movement or relocation during or immediately after an earthquake. Our analysis shows that even
767 during a large earthquake in mountainous terrain, landslide hazard is not ubiquitously high. A
768 significant fraction of the landscape has low landslide probability (<5% of the study area average) –
769 as much as 30% in Northridge and 33% in Nepal. This means that it is often possible to find locations
770 with lower landslide hazard. Landslide hazard is extremely granular in spatial terms, so that small
771 changes in location can make a big difference to exposure. The vast majority of locations (75% in
772 Nepal, 95% in Northridge) are within 1 km of areas of low landslide probability (<5% of the study
773 area average). Even smaller movements of 100 m or less, as might be possible during or immediately
774 after a large earthquake, can result in very large reductions in hazard.
775 Detailed analysis in the Northridge (Figure 7) and Nepal inventories shows that landslide hazard can
776 often be effectively reduced by moving from a slope to a ridge (e.g., from A to B in Figure 7), out of
777 a gully (e.g., from C to D), or downstream of a flatter area (e.g., from C to E). However, there is no
778 single answer to the question of where to move to reduce coseismic landslide hazard, since this
779 differs depending on the setting, the distance that can be travelled due to time or location constraints,
780 and on the chosen rule (e.g., skyline angle vs. hazard area). Given a 1 km radius of potential
781 movement, minimizing skyline angle involves moving upslope for ~75% of locations in Nepal but
782 only ~66% in Northridge. In some cases, knowing how far one can travel can be critical: if one may
783 only travel a short distance, moving upslope may be preferable (e.g., from C to D in Figure 7), while
784 if one could travel farther, moving downslope may offer greater hazard reduction (e.g., from C to F
785 or G).

Nat. Hazards Earth Syst. Sci. Discuss., https://doi.org/10.5194/nhess-2018-271
Manuscript under review for journal Nat. Hazards Earth Syst. Sci.
Discussion started: 13 November 2018

786 Landslide probability estimates for high hazard locations are broadly comparable between skyline
787 angle and hazard area metrics (e.g. Figure 7). However, different metrics emphasise different parts
788 of the landscape. Ridges consistently minimise skyline angle but may still have intermediate values
789 of hazard area if the ridge is sharp so that the local slope of the ridge itself is steep. Broad valley
790 floors consistently minimise hazard area, but may still have intermediate values of skyline angle if
791 the neighbouring slopes have sufficient relief. There are trade-offs between these metrics, and
792 further work is needed into how they might be combined to further reduce hazard.

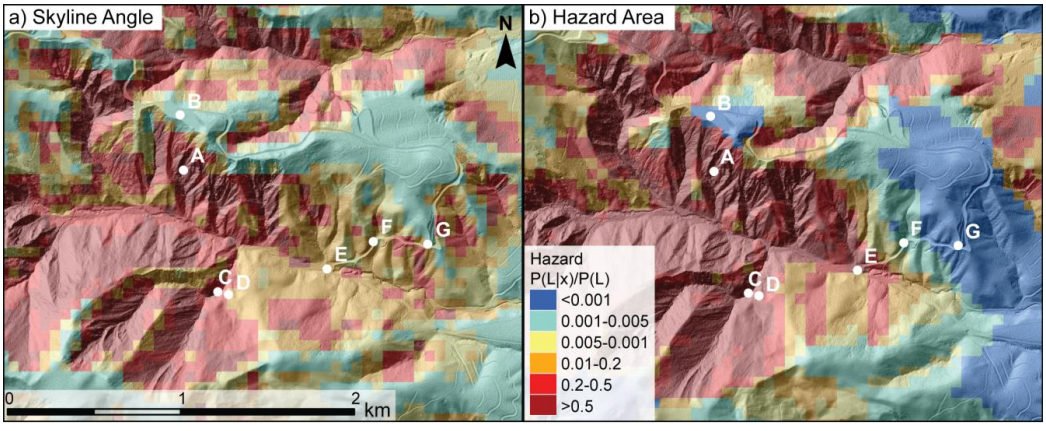

793

794 **Figure 7.** Example landslide hazard estimates derived from a) skyline angle and b) hazard area for
795 a small section of the Northridge study area. Colours reflect landslide hazard estimated from the
796 two methods, expressed as a fraction of the study area average hazard. Points labelled A-G in
797 white are example locations discussed in Section 7.4. Hazard estimates are overlain on shaded
798 relief from a 0.5 m resolution LiDAR DEM for context (source: NCALM, 2015,
799 DOI:10.5069/G9TB14V2).

800

801 **7.5 Caveats**

802 These rules should be combined with existing guidance, such as local knowledge and formal hazard
803 and risk information when that is available. The rules provide an evidence base that could be used,
804 for example, in infrastructure and land-use planning, identifying evacuation routes, and designing
805 contingency plans from individual to community level, where more detailed or formal technical advice
806 is not available. It is also important to note some caveats.

This analysis is purely focussed on coseismic landslide *hazard*, and thus it does not take into account the distribution of vulnerability: that is, the locations of people and infrastructure in these landscapes or how they might be differentially impacted by landslides. While one area may be more hazardous than another, the distribution of people and infrastructure may be such that risk is not actually increased. Further, our analysis is probabilistic, defining hazard as the probability of intersecting a landslide; thus, our rules identify locations where the landslide probability is lower, not where probability is zero. This means that it is possible for an alternate location chosen based on its lower landslide probability to be impacted by a landslide while the original higher-probability location is not. The choice of inventory will influence the specific results and, although we adjust for bulk shaking intensity by normalising conditional probability by bulk probability, differences between inventories are likely to remain (e.g., in spatial patterns of shaking intensity and their relation to topography). Rock type is a critical influence on landslide occurrence (Chen et al., 2012; Harp et al., 2016; Roback et al., 2018), but we have excluded it from our analysis because it is extremely difficult for an untrained observer to identify and to translate into meaningful estimates of material strength and thus landslide probability. While rock type is likely to influence the relationship between topography and landslide hazard (e.g., Chen et al., 2012) we expect the length scales over which this occurs to be long (order kilometres) relative to the other factors examined here.

Because the analysis is focussed on *coseismic landslide* hazard, it does not account for other sources of hazard, either associated with an earthquake (e.g., seismic amplification on ridges), or with other processes or events such as flooding. In some cases, following our rules in isolation might increase exposure to other hazards. For example, moving to ridge tops to minimise skyline angle might increase exposure to intense shaking due to seismic amplification; moving to valley floors that are occupied by large rivers, where hazard area is minimal, might increase exposure to fluvial flooding. We also have not considered the effects of landslide size or failure type, choosing instead to treat all landslides as representing an equivalent hazard. If landslide size or type shows a strong spatial dependence, then parts of the landscape may be preferentially impacted in ways that are not reflected by our rules. Finally, it is not yet clear how transferrable our conditional probability results are to rainfall-triggered landslides. For instance, stopping angles are likely to be lower for rainfall-triggered landslides where the failing mass is more highly saturated (e.g. Stock and Dietrich, 2003).

836 Similarly, in the case of rainfall-triggered landslides, initiation is likely to depend not only on slope
837 angle but also topographic control on saturation (e.g. Bellugi et al., 2011). Extending the analysis to
838 other triggering mechanisms is thus a future research need.
839
840 **8. Conclusions**
841 We have introduced a set of simple rules that can be used to identify, and thus potentially reduce,
842 exposure to earthquake-triggered landslides. We test a set of candidate predictors for their ability to
843 reproduce mapped landslide distributions from six recent earthquakes. Landslide hazard, defined as
844 the conditional probability of intersecting a landslide in one of the six earthquakes, increases
845 exponentially with local slope. Landslide hazard on hillslopes also increases with upslope
846 contributing area, suggesting that while ridges may be areas of preferential coseismic landslide
847 initiation, they are not the locations of highest coseismic landslide hazard due to downslope
848 movement of landslide material during runout. When accounting for both slope and upslope
849 contributing area, landslide hazard is highest for the highest area at a given slope or the highest
850 slope at a given area. Landslide hazard can be reduced by reducing local slope, even at the cost of
851 increased upslope contributing area, and especially at high slopes. Landslide hazard increases
852 exponentially with the skyline angle, and this simple, easily-measured, metric performs better than
853 slope or upslope contributing area for four of the six inventories. Hazard area, which accounts for
854 both landslide initiation and runout, offers the best predictive skill for all six inventories but is more
855 difficult to estimate in the field and requires estimation of two empirical parameters. Fortunately,
856 hazard area calculated with parameters that are averaged across all six study sites (initiation angle
857 of 39˚ and stopping angle of 10˚) performs only slightly worse than hazard area calculated with
858 optimised site-specific parameters, suggesting that the average parameters can be applied to other
859 inventories. These findings can be distilled into three simple rules:
860 1) Avoid steep (>10˚) channels with many steep (>39˚) areas that are upslope;
861 2) Minimise your maximum angle to the skyline; and
862 3) Minimise local slope, especially on steep slopes and even at the expense of increasing
863 upslope contributing area, but not at the expense of increasing skyline angle or hazard area.
864

Acknowledgements

This work was financially supported by grants from the NERC/ESRC Increasing Resilience to Natural Hazards programme (NE/J01995X/1) and the NERC/ESRC/NNSFC Increasing Resilience to Natural Hazards in China programme (NE/N012216/1). We thank: 1) colleagues at the National Society for Earthquake Technology-Nepal (NSET) who have helped to shape our thinking on landslide hazard and the challenge of risk communication; 2) those responsible for collecting the landslide inventories used in this study, particularly Neils Hovius and those that contributed their data to the ScienceBase-Catalog; and 3) William Dietrich and Neils Hovius for helpful comments on an earlier draft. LiDAR data acquisition and processing completed by the National Center for Airborne Laser Mapping (NCALM). NCALM funding provided by NSF's Division of Earth Sciences, Instrumentation and Facilities Program. EAR-1043051.

References

Abbott, L.D., Silver, E.A., Anderson, R.S., Smith, R., Ingle, J.C., Kling, S.A., Haig, D., Small, E., Galewsky, J. and Sliter, W.S.: Measurement of tectonic surface uplift rate in a young collisional mountain belt. *Nature*, *385*(6616), pp.501-507. 1997.

Alexander, D.: Vulnerability to landslides. In *Landslide Hazard and Risk. Wiley, Chichester*, pp.175-198. 2005.

Atwater B.F., Cisternas M.V., Bourgeois J., Dudley W.C., Hendley J.W., and Stauffer P.H.: Surviving a tsunami--lessons from Chile, Hawaii, and Japan (No. 1187). Geological Survey (USGS). 1999.

Bellugi, D., Dietrich, W.E., Stock, J., McKean, J., Kazian, B. and Hargrove, P.: Spatially explicit shallow landslide susceptibility mapping over large areas. *Proceedings of the 5th International Conference on Debris-Flow Hazards Mitigation: Mechanics, Prediction and Assessment, Italian Journal of Engineering Geology and Environment. 759-768*. DOI: 10.4408/IJEGE.2011-03.B-045. 2011.

Benda, L.E. and Cundy, T.W.: Predicting deposition of debris flows in mountain channels. *Canadian Geotechnical Journal*, *27*(4), pp.409-417. 1990.

893 Blöthe, J.H., Korup, O. and Schwanghart, W.: Large landslides lie low: Excess topography in the
894 Himalaya-Karakoram ranges. *Geology*, *43*(6), pp.523-526. 2015.
895 Bookhagen, B. and Burbank, D.W.: Topography, relief, and TRMM-derived rainfall variations along
896 the Himalaya. *Geophysical Research Letters*, *33*(8). 2006.
897 Briggs, J.: The use of indigenous knowledge in development: problems and challenges. *Progress*
898 *in Development Studies*, 5(2): 99-114. 2005.
899 Burchfiel, B.C., Zhiliang, C., Yupinc, L. and Royden, L.H.: Tectonics of the Longmen Shan and
900 adjacent regions, central China. *International Geology Review*, *37*(8), pp.661-735. 1995.
901 Chen, X.L., Ran, H.L. and Yang, W.T.: Evaluation of factors controlling large earthquake-induced
902 landslides by the Wenchuan earthquake. *Natural Hazards and Earth System Sciences*, *12*(12),
903 pp.3645-3657. 2012.
904 Chi, W.C., Dreger, D. and Kaverina, A.: Finite-source modeling of the 1999 Taiwan (Chi-Chi)
905 earthquake derived from a dense strong-motion network. *Bulletin of the Seismological Society of*
906 *America*, *91*(5), pp.1144-1157. 2001.
907 Churches, C.E., Wampler, P.J., Sun, W. and Smith, A.J.: Evaluation of forest cover estimates for
908 Haiti using supervised classification of Landsat data. *International Journal of Applied Earth*
909 *Observation and Geoinformation*, *30*, pp.203-216. 2014.
910 Claessens, L., Heuvelink, G.B.M., Schoorl, J.M. and Veldkamp, A.: DEM resolution effects on
911 shallow landslide hazard and soil redistribution modelling. *Earth Surface Processes and*
912 *Landforms*, *30*(4), pp.461-477. 2005.
913 Corominas, J.: The angle of reach as a mobility index for small and large landslides. *Canadian*
914 *Geotechnical Journal*, *33*(2), pp.260-271. 1996.
915 Colburn, I.P., Saul, L.E.R. and Almgren, A.A.: The Chatsworth Formation: a new formation name
916 for the Upper Cretaceous strata of the Simi Hills, California. 1981.
917 Craddock, W.H., Burbank, D.W., Bookhagen, B. and Gabet, E.J.: Bedrock channel geometry along
918 an orographic rainfall gradient in the upper Marsyandi River valley in central Nepal. *Journal of*
919 *Geophysical Research: Earth Surface*, *112*(F3). 2007.

920 Dadson, S.J., Hovius, N., Chen, H., Dade, W.B., Hsieh, M.L., Willett, S.D., Hu, J.C., Horng, M.J.,
921 Chen, M.C., Stark, C.P. and Lague, D.: Links between erosion, runoff variability and seismicity in
922 the Taiwan orogen. *Nature*, *426*(6967), pp.648-651. 2003.
923 Dai, F.C., Xu, C., Yao, X., Xu, L., Tu, X.B. and Gong, Q.M.: Spatial distribution of landslides
924 triggered by the 2008 Ms 8.0 Wenchuan earthquake, China. *Journal of Asian Earth Sciences*,
925 *40*(4), pp.883-895. 2011.
926 Datta, A., Sigdel, S., Oven, K., Rosser, N., Densmore, A., Rijal, S.: The role of scientific evidence
927 during the 2015 Nepal earthquake relief efforts. *Overseas Development Institute: London, UK*.:
928 2018.
929 Davies, H.L., Lock, J., Tiffin, D.L., Honza, E., Okuda, Y., Murakami, F. and Kisimoto, K.:
930 Convergent tectonics in the Huon Peninsula region, Papua New Guinea. *Geo-Marine Letters*, *7*(3),
931 pp.143-152. 1987.
932 Densmore, A.L., Ellis, M.A. and Anderson, R.S.: Landsliding and the evolution of normal-fault-
933 bounded mountains. *Journal of geophysical research: solid earth*, *103*(B7), pp.15203-15219. 1998.
934 Densmore, A.L. and Hovius, N.: Topographic fingerprints of bedrock landslides. *Geology*, *28*(4),
935 pp.371-374. 2000.
936 Densmore, A.L., Ellis, M.A., Li, Y., Zhou, R., Hancock, G.S. and Richardson, N.: Active tectonics of
937 the Beichuan and Pengguan faults at the eastern margin of the Tibetan Plateau. *Tectonics*, *26*(4).
938 2007.
939 Dietrich, W.E. and Sitar, N.: Geoscience and geotechnical engineering aspects of debris-flow
940 hazard assessment. In *Debris-flow hazards mitigation: Mechanics, prediction, and assessment* (pp.
941 656-676). ASCE. 1997.
942 Dransch, D., Rotzoll, H. and Poser, K.: The contribution of maps to the challenges of risk
943 communication to the public. *International Journal of Digital Earth*, *3*(3), pp.292-311. 2010.
944 Elliott, J.R., Jolivet, R., González, P.J., Avouac, J.P., Hollingsworth, J., Searle, M.P. and Stevens,
945 V.L.: Himalayan megathrust geometry and relation to topography revealed by the Gorkha
946 earthquake. *Nature Geoscience*, *9*(2), pp.174-180. 2016.

947 Escuder-Viruete, J., Pérez-Estaún, A., Contreras, F., Joubert, M., Weis, D., Ullrich, T.D. and
948 Spadea, P.: Plume mantle source heterogeneity through time: Insights from the Duarte Complex,
949 Hispaniola, northeastern Caribbean. *Journal of Geophysical Research: Solid Earth*, *112*(B4). 2007.
950 Fannin, R.J. and Wise, M.P.: An empirical-statistical model for debris flow travel
951 distance. *Canadian Geotechnical Journal*, *38*(5), pp.982-994. 2001.
952 Fell, R., Ho, K.K., Lacasse, S. and Leroi, E.: A framework for landslide risk assessment and
953 management. *Landslide risk management*, pp.3-25. 2005.
954 George, D.L. and Iverson, R.M.: A depth-averaged debris-flow model that includes the effects of
955 evolving dilatancy: 2. Numerical predictions and experimental tests *Proc. R. Soc. Lond. Ser. A*, 470
956 p. 20130820. 2014.
957 Frattini, P., Crosta, G. and Carrara, A.: Techniques for evaluating the performance of landslide
958 susceptibility models. *Engineering geology*, *111*(1-4), pp.62-72. 2010.
959 Geller, R.J.: Earthquake prediction: a critical review. *Geophysical Journal International*, *131*(3),
960 pp.425-450. 1997.
961 Gigerenzer, G.: Why heuristics work. *Perspectives on psychological science*, *3*(1), pp.20-29. 2008.
962 Godard, V., Lavé, J., Carcaillet, J., Cattin, R., Bourlès, D. and Zhu, J.: Spatial distribution of
963 denudation in Eastern Tibet and regressive erosion of plateau margins. *Tectonophysics*, *491*(1),
964 pp.253-274. 2010.
965 Godard, V., Bourlès, D.L., Spinabella, F., Burbank, D.W., Bookhagen, B., Fisher, G.B., Moulin, A.
966 and Léanni, L.: Dominance of tectonics over climate in Himalayan denudation. *Geology*, *42*(3),
967 pp.243-246. 2014.
968 Gorum, T., Fan, X., van Westen, C.J., Huang, R.Q., Xu, Q., Tang, C. and Wang, G.: Distribution
969 pattern of earthquake-induced landslides triggered by the 12 May 2008 Wenchuan
970 earthquake. *Geomorphology*, *133*(3), pp.152-167. 2011.
971 Gorum, T., van Westen, C.J., Korup, O., van der Meijde, M., Fan, X. and van der Meer, F.D.:
972 Complex rupture mechanism and topography control symmetry of mass-wasting pattern, 2010
973 Haiti earthquake. *Geomorphology*, *184*, pp.127-138. 2013.

974 Gorum, T., Korup, O., van Westen, C.J., van der Meijde, M., Xu, C. and van der Meer, F.D.: Why
975 so few? Landslides triggered by the 2002 Denali earthquake, Alaska. *Quaternary Science*
976 *Reviews*, *95*, pp.80-94. 2014.
977 Griffith, G.E., Omernik, J.M., Smith, D.W., Cook, T.D., Tallyn, E., Moseley, K., and Johnson, C.B.:
978 Ecoregions of California (poster): U.S. Geological Survey Open-File Report 2016–1021, with map,
979 scale 1:1,100,000, http://dx.doi.org/10.3133/ofr20161021. 2016.
980 Guillard-Gonçalves, C., Zêzere, J.L., Pereira, S. and Garcia, R.A.C.: Assessment of physical
981 vulnerability of buildings and analysis of landslide risk at the municipal scale: application to the
982 Loures municipality, Portugal.*Natural Hazards & Earth System Sciences*, *16*(2). 2016.
983 Hancock, G.R. and Evans, K.G.: Channel head location and characteristics using digital elevation
984 models. *Earth Surface Processes and Landforms*, *31*(7), pp.809-824. 2006.
985 Harp, E.L., Wilson, R.C. and Wieczorek, G.F.: *Landslides from the February 4, 1976, Guatemala*
986 *earthquake*(No. 551.3 HAR). US Government Printing Office. 1981.
987 Harp, E.L. and Jibson, R.W.: Landslides triggered by the 1994 Northridge, California,
988 earthquake. *Bulletin of the Seismological Society of America*, *86*(1B), pp.S319-S332. 1996.
989 Harp, E.L., Jibson, R.W., and Schmitt, R.G.: Map of landslides triggered by the January 12, 2010,
990 Haiti earthquake: U.S. Geological Survey Scientific Investigations Map 3353, 15 p., 1 sheet, scale
991 1:150,000, http://dx.doi.org/10.3133/sim3353. 2016.
992 Harp, E.L., Jibson, R.W., Schmitt, R.G.: Map of landslides triggered by the January 12, 2010, Haiti
993 earthquake, https://doi.org/10.5066/F7C827SR, in Schmitt, R.G., Tanyas, Hakan, Nowicki Jessee,
994 M.A., Zhu, J., Biegel, K.M., Allstadt, K.E., Jibson, R.W., Thompson, E.M., van Westen, C.J., Sato,
995 H.P., Wald, D.J., Godt, J.W., Gorum, Tolga, Xu, Chong, Rathje, E.M., Knudsen, K.L., 2017, An
996 Open Repository of Earthquake-triggered Ground Failure Inventories, U.S. Geological Survey data
997 release collection, accessed July 18, 2018, at https://doi.org/10.5066/F7H70DB4. 2017.
998 Hauksson, E., Jones, L.M. and Hutton, K.: The 1994 Northridge earthquake sequence in California:
999 Seismological and tectonic aspects. *Journal of Geophysical Research: Solid Earth*, *100*(B7),
1000 pp.12335-12355. 1995.
1001 Heim, A.: *Bergsturz und menschenleben* (No. 20). Fretz & Wasmuth. 1932.

1002 Hodges, K.V., Parrish, R.R. and Searle, M.P. Tectonic evolution of the central Annapurna range,
1003 Nepalese Himalayas. *Tectonics*, *15*(6), pp.1264-1291. 1996.
1004 Hovius, N., Stark, C.P., Tutton, M.A. and Abbott, L.D.: Landslide-driven drainage network evolution
1005 in a pre-steady-state mountain belt: Finisterre Mountains, Papua New Guinea. *Geology*, *26*(12),
1006 pp.1071-1074. 1998.
1007 Huang, R. and Fan, X.: The landslide story. *Nature Geoscience*, *6*(5), pp.325-326. 2013.
1008 Hunter, G. and Fell, R.: Travel distance angle for" rapid" landslides in constructed and natural soil
1009 slopes. *Canadian Geotechnical Journal*, *40*(6), pp.1123-1141. 2003.
1010 Jaboyedoff, M., Baillifard, F., Couture, R., Locat, J. and Locat, P.: Toward preliminary hazard
1011 assessment using DEM topographic analysis and simple mechanical modeling by means of
1012 sloping local base level. *Landslides: evaluation and stabilization. Balkema, Taylor & Francis Group,*
1013 *London*, pp.199-206. 2004.
1014 Keefer, D.K.: Statistical analysis of an earthquake-induced landslide distribution—the 1989 Loma
1015 Prieta, California event. *Engineering geology*, *58*(3), pp.231-249. 2000.
1016 Libohova, Z., Wysocki, D., Schoeneberger, P., Reinsch, T., Kome, C., Rolfes, T., Jones, N.,
1017 Monteith, S. and Matos, M.: Soils and climate of Cul de Sac Valley, Haiti: A soil water and
1018 geomorphology perspective. *Journal of Soil and Water Conservation*, *72*(2), pp.91-101. 2017.
1019 Kennedy, I.T., Petley, D.N., Williams, R. and Murray, V.: A systematic review of the health impacts
1020 of mass Earth movements (landslides). *PLoS currents*, 7. 2015.
1021 Kahneman, D. and Klein, G.: Conditions for intuitive expertise: a failure to disagree. *American*
1022 *Psychologist*, *64*(6), p.515. 2009.
1023 Klose, M., Maurischat, P. and Damm, B.: Landslide impacts in Germany: A historical and
1024 socioeconomic perspective. *Landslides*, *13*(1), pp.183-199. 2016.
1025 Kritikos, T., Robinson, T.R. and Davies, T.R.: Regional coseismic landslide hazard assessment
1026 without historical landslide inventories: A new approach. *Journal of Geophysical Research: Earth*
1027 *Surface*, *120*(4), pp.711-729. 2015.
1028 Lavé, J. and Avouac, J.P.: Active folding of fluvial terraces across the Siwaliks Hills, Himalayas of
1029 central Nepal. *Journal of Geophysical Research: Solid Earth*, *105*(B3), pp.5735-5770. 2000.

1030 Lavé, J. and Burbank, D.: Denudation processes and rates in the Transverse Ranges, southern
1031 California: Erosional response of a transitional landscape to external and anthropogenic forcing.
1032 *Journal of Geophysical Research: Earth Surface*, *109*(F1). 2004.
1033 Lee, E.M. and Jones, D.K.: *Landslide risk assessment*. Thomas Telford. 2004.
1034 Lee, S. and Sambath, T.: Landslide susceptibility mapping in the Damrei Romel area, Cambodia
1035 using frequency ratio and logistic regression models. *Environmental Geology*, *50*(6), pp.847-855.
1036 2006.
1037 Lee, S. and Pradhan, B.: Landslide hazard mapping at Selangor, Malaysia using frequency ratio
1038 and logistic regression models. *Landslides*, *4*(1), pp.33-41. 2007.
1039 Lee, W.H.K., Shin, T.C., Kuo, K.W., Chen, K.C. and Wu, C.F.: CWB free-field strong-motion data
1040 from the 21 September Chi-Chi, Taiwan, earthquake. *Bulletin of the seismological society of*
1041 *America*, *91*(5), pp.1370-1376. 2001.
1042 Li, G., West, A.J., Densmore, A.L., Jin, Z., Parker, R.N. and Hilton, R.G.: Seismic mountain
1043 building: Landslides associated with the 2008 Wenchuan earthquake in the context of a
1044 generalized model for earthquake volume balance. *Geochemistry, Geophysics, Geosystems*,
1045 *15*(4), pp.833-844. 2014.
1046 Li, G., West, A.J., Densmore, A.L., Hammond, D.E., Jin, Z., Zhang, F., Wang, J. and Hilton, R.G.:
1047 Connectivity of earthquake-triggered landslides with the fluvial network: Implications for landslide
1048 sediment transport after the 2008 Wenchuan earthquake. *Journal of Geophysical Research: Earth*
1049 *Surface*, *121*(4), pp.703-724. 2016.
1050 Li, X., Zhou, Z., Yu, H., Wen, R., Lu, D., Huang, M., Zhou, Y. and Cu, J.: Strong motion
1051 observations and recordings from the great Wenchuan Earthquake. *Earthquake Engineering and*
1052 *Engineering Vibration*, *7*(3), pp.235-246. 2008.
1053 Lin, G.W., Chen, H., Hovius, N., Horng, M.J., Dadson, S., Meunier, P. and Lines, M.: Effects of
1054 earthquake and cyclone sequencing on landsliding and fluvial sediment transfer in a mountain
1055 catchment. *Earth Surface Processes and Landforms*, *33*(9), pp.1354-1373. 2008.
1056 Lin, M.L., Wang, K.L. and Chen, T.C.: September. Characteristics of the slope failure caused by
1057 Chi-Chi earthquake. In *International workshop on annual commemoration of Chi-Chi earthquake*
1058 *(III): Taipei, National Center for Research on Earthquake Engineering* (pp. 199-209). 2000.

1059 Liu-Zeng, J., Wen, L., Oskin, M. and Zeng, L.: Focused modern denudation of the Longmen Shan
1060 margin, eastern Tibetan Plateau. *Geochemistry, Geophysics, Geosystems*, *12*(11). 2011.
1061 Lupker, M., Blard, P.H., Lave, J., France-Lanord, C., Leanni, L., Puchol, N., Charreau, J. and
1062 Bourlès, D.: 10 Be-derived Himalayan denudation rates and sediment budgets in the Ganga
1063 basin. *Earth and Planetary Science Letters*, *333*, pp.146-156. 2012.
1064 MacKinnon, J.R. ed.: *Protected areas systems review of the Indo-Malayan realm*. Asian Bureau for
1065 Conservation. 1997.
1066 McCammon, I.: Heuristic traps in recreational avalanche accidents: Evidence and implications.
1067 Avalanche News, 68(1), pp.1-10. 2004.
1068 Meigs, A., Brozovic, N. and Johnson, M.L.: Steady, balanced rates of uplift and erosion of the
1069 Santa Monica Mountains, California. *Basin Research*, *11*(1), pp.59-73. 1999.
1070 Mercier de Lépinay, B.M., Deschamps, A., Klingelhoefer, F., Mazabraud, Y., Delouis, B., Clouard,
1071 V., Hello, Y., Crozon, J., Marcaillou, B., Graindorge, D. and Vallée, M.: The 2010 Haiti earthquake:
1072 A complex fault pattern constrained by seismologic and tectonic observations. *Geophysical*
1073 *Research Letters*, *38*(22). 2011.
1074 Mertens, K., Jacobs, L., Maes, J., Kabaseke, C., Maertens, M., Poesen, J., Kervyn, M. and
1075 Vranken, L.: The direct impact of landslides on household income in tropical regions: A case study
1076 from the Rwenzori Mountains in Uganda. *Science of the Total Environment*, *550*, pp.1032-1043.
1077 2016.
1078 Meunier, P., Hovius, N. and Haines, A.J.: Regional patterns of earthquake-triggered landslides and
1079 their relation to ground motion. *Geophysical Research Letters*, *34*(20). 2007.
1080 Meunier, P., Hovius, N. and Haines, J.A.: Topographic site effects and the location of earthquake
1081 induced landslides. *Earth and Planetary Science Letters*, *275*(3), pp.221-232. 2008.
1082 Mills, J.W. and Curtis, A.: Geospatial approaches for disease risk communication in marginalized
1083 communities. *Progress in community health partnerships: research, education, and action*, *2*(1),
1084 pp.61-72. 2008.
1085 Montgomery, D.R.: Compressional uplift in the central California Coast Ranges. *Geology*, *21*(6),
1086 pp.543-546. 1993.

1087 Montgomery, D.R. and Foufoula-Georgiou, E.: Channel network source representation using digital
1088 elevation models. *Water Resources Research*,*29*(12), pp.3925-3934. 1993.
1089 Montgomery, D.R. and Dietrich, W.E.: A physically based model for the topographic control on
1090 shallow landsliding. *Water resources research*, *30*(4), pp.1153-1171. 1994.
1091 Moughtin, C.: Barkulti in the Yasmin valley: A study of traditional settlement form as a response to
1092 environmental hazard. The International Karakorum Project. Vol. 2, Proceedings of the
1093 international conference held at the Royal Geographical Society, London. K. J. Miller. Cambridge:
1094 Cambridge University Press: 307-322. 1984.
1095 National Atlas of the United States: *United States Average Annual Precipitation, 1990-2009, Map*,
1096 Reston, VA. https://catalog.data.gov/dataset/united-states-average-annual-precipitation-1990-
1097 2009-direct-download. 2011.
1098 *NOAA: Online Weather Data*: http://w2.weather.gov/climate/xmacis.php?wfo=sgx. *National*
1099 *Oceanic and Atmospheric Administration*. *Retrieved 2017-10-30. 2017.*
1100 NCALM: National Centre for Airborne Laser Mapping. *Santa Clarita Topography, Airborne Lidar*
1101 *Data Acquired 06/17/2015*. DOI:10.5069/G9TB14V2. 2015.
1102 Olson, D.M., Dinerstein, E., Wikramanayake, E.D., Burgess, N.D., Powell, G.V., Underwood, E.C.,
1103 D'amico, J.A., Itoua, I., Strand, H.E., Morrison, J.C. and Loucks, C.J.: Terrestrial Ecoregions of the
1104 World: A New Map of Life on Earth A new global map of terrestrial ecoregions provides an
1105 innovative tool for conserving biodiversity. *BioScience*, *51*(11), pp.933-938. 2001.
1106 Ouimet, W.B., Whipple, K.X. and Granger, D.E.: Beyond threshold hillslopes: Channel adjustment
1107 to base-level fall in tectonically active mountain ranges. *Geology*, *37*(7), pp.579-582. 2009.
1108 Parise, M. and Jibson, R.W.: A seismic landslide susceptibility rating of geologic units based on
1109 analysis of characteristics of landslides triggered by the 17 January, 1994 Northridge, California
1110 earthquake. *Engineering geology*, *58*(3), pp.251-270. 2000.
1111 Parker, R.N., Rosser, N.J. and Hales, T.C.: Spatial prediction of earthquake-induced landslide
1112 probability. *Nat. Hazards Earth Syst. Sci. Discuss., https://doi. org/10.5194/nhess-2017-193, in*
1113 *review*. 2017.
1114 Paijmans, K., 1975. Explanatory notes to the vegetation map of Papua New Guinea.

1115 Peel, M.C., Finlayson, B.L. and McMahon, T.A.: Updated world map of the Köppen-Geiger climate
1116 classification. *Hydrology and earth system sciences discussions*, *4*(2), pp.439-473. 2007.
1117 Pubellier, M., Mauffret, A., Leroy, S., Vila, J.M. and Amilcar, H.: Plate boundary readjustment in
1118 oblique convergence: Example of the Neogene of Hispaniola, Greater Antilles. *Tectonics*, *19*(4),
1119 pp.630-648. 2000.
1120 Petley, D.: Global patterns of loss of life from landslides. *Geology*,*40*(10), pp.927-930. 2012.
1121 Pradhan, B.: A comparative study on the predictive ability of the decision tree, support vector
1122 machine and neuro-fuzzy models in landslide susceptibility mapping using GIS. *Computers &*
1123 *Geosciences*, *51*, pp.350-365. 2013.
1124 Quinn, P., Beven, K., Chevallier, P. and Planchon, O.: The prediction of hillslope flow paths for
1125 distributed hydrological modelling using digital terrain models. *Hydrological processes*, *5*(1), pp.59-
1126 79. 1991.
1127 Roback, K., Clark, M.K., West, A.J., Zekkos, D., Li, G., Gallen, S.F., Chamlagain, D. and Godt,
1128 J.W.: The size, distribution, and mobility of landslides caused by the 2015 M w 7.8 Gorkha
1129 earthquake, Nepal. *Geomorphology*. 2017.
1130 Roering, J.J., Perron, J.T. and Kirchner, J.W.: Functional relationships between denudation and
1131 hillslope form and relief. *Earth and Planetary Science Letters*, *264*(1-2), pp.245-258. 2007.
1132 Schwanghart, W. and Kuhn, N.J.: TopoToolbox: A set of Matlab functions for topographic
1133 analysis. *Environmental Modelling & Software*, *25*(6), pp.770-781. 2010.
1134 Searle, M.P. and Godin, L.: The South Tibetan detachment and the Manaslu leucogranite: A
1135 structural reinterpretation and restoration of the Annapurna-Manaslu Himalaya, Nepal. *The Journal*
1136 *of Geology*, *111*(5), pp.505-523. 2003.
1137 Sen, G., Hickey-Vargas, R., Waggoner, D.G. and Maurrasse, F.: Geochemistry of basalts from the
1138 Dumisseau Formation, southern Haiti: implications for the origin of the Caribbean Sea crust. *Earth*
1139 *and Planetary Science Letters*, *87*(4), pp.423-437. 1988.
1140 Shaw, R., Uy, N. and Baumwoll, J.: Indigenous knowledge for disaster risk reduction: Good
1141 practices and lessons learned from experiences in the Asia-Pacific Region. *United Nations*
1142 *International Strategy for Disaster Reduction: Bangkok*. 2008.

1143 Shin, T.C. and Teng, T.L.: An overview of the 1999 Chi-Chi, Taiwan, earthquake. *Bulletin of the*
1144 *Seismological Society of America*, *91*(5), pp.895-913. 2001.
1145 Singh, J.S. and Singh, S.P.: Forest vegetation of the Himalaya. *The Botanical Review*, *53*(1),
1146 pp.80-192. 1987.
1147 Stevens, C., McCaffrey, R., Silver, E.A., Sombo, Z., English, P. and Van der Kevie, J.: Mid-crustal
1148 detachment and ramp faulting in the Markham Valley, Papua New Guinea. *Geology*, *26*(9), pp.847-
1149 850. 1998.
1150 Stock, J. and Dietrich, W.E.: Valley incision by debris flows: Evidence of a topographic
1151 signature. *Water Resources Research*, *39*(4). 2003.
1152 Taylor, D.W.: *Stability of earth slopes* (pp. 1925-1940). Wright & Potter print. 1937.
1153 Thompson, M.A., Lindsay, J.M. and Gaillard, J.C.: The influence of probabilistic volcanic hazard
1154 map properties on hazard communication.*Journal of Applied Volcanology*, *4*(1), p.1. 2015.
1155 Tibaldi, A., Ferrari, L. and Pasquarè, G.: Landslides triggered by earthquakes and their relations
1156 with faults and mountain slope geometry: an example from Ecuador. *Geomorphology*, *11*(3),
1157 pp.215-226. 1995.
1158 Travis, M.R., Iverson, W.D., Eisner, G.H. and Johnson, C.G., VIEWIT: computation of seen areas,
1159 slope, and aspect for land-use planning. *Gen Tech Rep PSW Pac Southwest For Range Exp Stn*
1160 *USDA For Serv*. 1975.
1161 Tsutsumi, H. and Yeats, R.S.: Tectonic setting of the 1971 Sylmar and 1994 Northridge
1162 earthquakes in the San Fernando Valley, California. *Bulletin of the Seismological Society of*
1163 *America*, *89*(5), pp.1232-1249. 1999.
1164 Twigg, J., Lovell, E., Schofield, H., Miranda Morel, L., Flinn, B., Sargeant, S., Finlayson, A.,
1165 Dijkstra, T., Stephenson, V., Albuerne, A. and Rossetto, T.: Self-recovery from disasters: an
1166 interdisciplinary perspective. *Overseas Development Institute: London, UK*. 2017.
1167 Volkwein, A., Schellenberg, K., Labiouse, V., Agliardi, F., Berger, F., Bourrier, F., Dorren, L.K.,
1168 Gerber, W. and Jaboyedoff, M.: Rockfall characterisation and structural protection-a
1169 review. *Natural Hazards and Earth System Sciences*, *11*, pp.p-2617. 2011.
1170 von Ruette, J., Lehmann, P. and Or, D. Linking rainfall-induced landslides with predictions of debris
1171 flow runout distances. *Landslides*, *13*(5), pp.1097-1107. 2016.

1172 Wald, D.J. and Heaton, T.H.: *A dislocation model of the 1994 Northridge, California, earthquake*
1173 *determined from strong ground motions* (No. 94-278). US Geological Survey. 1994.
1174 Wang, W.N., Wu, H.L., Nakamura, H., Wu, S.C., Ouyang, S. and Yu, M.F.: Mass movements
1175 caused by recent tectonic activity: the 1999 Chi-chi earthquake in central Taiwan. *Island Arc*, *12*(4),
1176 pp.325-334. 2003.
1177 Xu, C., Shyu, J.B.H. and Xu, X.: Landslides triggered by the 12 January 2010 Port-au-Prince, Haiti,
1178 Mw= 7.0 earthquake: visual interpretation, inventory compiling, and spatial distribution statistical
1179 analysis. *Natural Hazards and Earth System Sciences*, *14*(7), p.1789. 2014.
1180 Xu, C., Xu, X., Dai, F. and Saraf, A.K.: Comparison of different models for susceptibility mapping of
1181 earthquake triggered landslides related with the 2008 Wenchuan earthquake in China. *Computers*
1182 *& Geosciences*, *46*, pp.317-329. 2012.
1183 Xu, C., Xu, X. and Yu, G.: Landslides triggered by slipping-fault-generated earthquake on a
1184 plateau: an example of the 14 April 2010, Ms 7.1, Yushu, China earthquake. *Landslides*, *10*(4),
1185 pp.421-431. 2013.
1186 Xu, X., Wen, X., Yu, G., Chen, G., Klinger, Y., Hubbard, J. and Shaw, J.: Coseismic reverse-and
1187 oblique-slip surface faulting generated by the 2008 Mw 7.9 Wenchuan earthquake,
1188 China. *Geology*, *37*(6), pp.515-518. 2009.
1189 Wu, C.C. and Kuo, Y.H.: Typhoons affecting Taiwan: Current understanding and future
1190 challenges. *Bulletin of the American Meteorological Society*, *80*(1), pp.67-80. 1999.
1191 Yilmaz, I.: Landslide susceptibility mapping using frequency ratio, logistic regression, artificial
1192 neural networks and their comparison: a case study from Kat landslides (Tokat—Turkey).
1193 *Computers & Geosciences*, *35*(6), pp.1125-1138. 2009.
1194 Yin, K.L. and Yan, T.Z.: July. Statistical prediction model for slope instability of metamorphosed
1195 rocks. In *Proceedings of the 5th international symposium on landslides, Lausanne, Switzerland*
1196 (Vol. 2, pp. 1269-1272). AA Balkema Rotterdam, The Netherlands. 1988.
1197 Yu, G., Tang, L., Yang, X., Ke, X. and Harrison, S.P.: Modern pollen samples from alpine
1198 vegetation on the Tibetan Plateau. *Global Ecology and Biogeography*, *10*(5), pp.503-519. 2001.